MGPB

Changes of thermocline depth at the Sumba Island offshore based on planktonic foraminiferal assemblages and its implication to eutrophication since the Last Deglaciation (~18 ka BP): a preliminary study

Rudarsko-geološko-naftni zbornik
(The Mining-Geology-Petroleum Engineering Bulletin)
UDC: 56; 550.8; 551.58; 551.8
DOI: 10.17794/rgn.2021.3.3

Original scientific paper

Ryan Dwi Wahyu Ardi[1,2]; Aswan[1]; Khoiril Anwar Maryunani[1]; Eko Yulianto[3]; Purna Sulastya Putra[1,3]; Septriono Hari Nugroho[1,3]

[1] Geological Engineering Study Program, Faculty of Earth Science and Technology, Institut Teknologi Bandung, Jl. Ganesha No. 10 Bandung 40132

[2] Agrotechnology Study Program, Faculty of Science and Technology, Universitas Nahdlatul Ulama Purwokerto, Jl. Sultan Agung No. 42 Purwokerto 53144

[3] Research Center for Geotechnology, Indonesian Institute of Sciences, Jl. Sangkuriang Kompleks LIPI Bandung 40135
https://orcid.org/0000-0002-4417-5852 (PSP)

Abstract

Changes of the thermocline depth (DOT) at the Sumba Island offshore are not well-known compared to the DOT changes in the Timor Sea, the main exit passage of the Indonesian Through-flow (ITF). Planktonic foraminiferal assemblages in cores collected from the southwest Sumba offshore (ST08) and Sumba Strait (ST12, ST13, and ST14) were used as a tool to infer the DOT and paleoproductivity changes at the Sumba Island offshore. The DOT changes were indicated from the thermocline and mixed layer dwellers' relative abundance while the paleoproductivity changes were indicated from the relative abundance of *Neogloboquadrina dutertrei*. This study suggests a contrast between the DOT pattern at the Sumba Island offshore and the DOT pattern in the Timor Sea during the Last Deglaciation–Holocene. The contrast DOT pattern indicated that the multi-millennial changes of the Australian-Indonesian monsoon (AIM) during the Last Deglaciation–Holocene were the main factors behind the DOT changes in this region while the effects of *El Niño* Southern Oscillation (ENSO) –like, Indian Ocean Dipole (IOD) –like, and ITF to DOT changes were minimal. Paleoproductivity enhancement at the Sumba Island offshore was not solely related to the monsoon-driven coastal upwelling intensification, which resulted in the DOT shoaling and eutrophic condition. The increase of nutrient availability in surface water due to river runoff increase and changes in the lifted water mass nature were also able to enhance productivity in this region.

Keywords:
Australian–Indonesian monsoon; applied micropaleontology; Indonesian Throughflow; Lesser Sunda Islands; paleoceanography

1. Introduction

The Depth of Thermocline (DOT), which is the distance between the upper limit of the thermocline layer and the ocean surface (**Lana et al., 2017**), is one of the most studied parameters in paleoceanographic studies (**Spooner et al., 2005; Ding et al., 2013; Kwiatkowski et al., 2015**). The study of the DOT changes is important due to their association with the variation of upwelling intensity and marine productivity (**Brasier, 1995; Müller and Opdyke, 2000; Holbourn et al., 2005**). The increase of the upwelling intensity is indicated in the shoaling of the DOT which triggers the eutrophication process as the nutrient-rich cool water layer reaches the photic zone (**Brasier, 1995; Susanto et al., 2001**). This condition is also known as eutrophic, which is associated with the regime of higher marine productivity (**Brasier, 1995; Spooner et al., 2005; Andruleit et al., 2008**). On the other hand, the condition when the nutrient-rich cool water layer does not reach the photic zone is known as oligotrophic, associated with the regime of lower marine productivity (**Brasier, 1995; Spooner et al., 2005; Andruleit et al., 2008**).

The DOT in the Indonesian region varies spatially with the shallower DOT in its western part and the deeper DOT in its eastern part (**Lana et al., 2017**). The shallower DOT in western Indonesia is associated with the development of coastal upwelling at the south Sumatra offshore–Lesser Sunda Islands, also known as the Java upwelling region, especially during the Australia-Indonesian winter monsoon (AIWM) (**Susanto et al., 2001, 2006; Andruleit et al., 2008**). In eastern Indonesia, the upwelling-related DOT shoaling is hindered by the maximum flow of ITF's surface water, and as a result, the DOT is relatively deeper than in western Indonesia (**Gordon and Fine, 1996; Lana et al., 2017**). On the glacial-interglacial scale, changes in the DOT are also related to the changes of the Australia-Indonesian monsoon (AIM) configuration and the hydrographic changes

Corresponding author: Ryan Dwi Wahyu Ardi
dwa.ryan@students.itb.ac.id; dwa.ryan@gmail.com

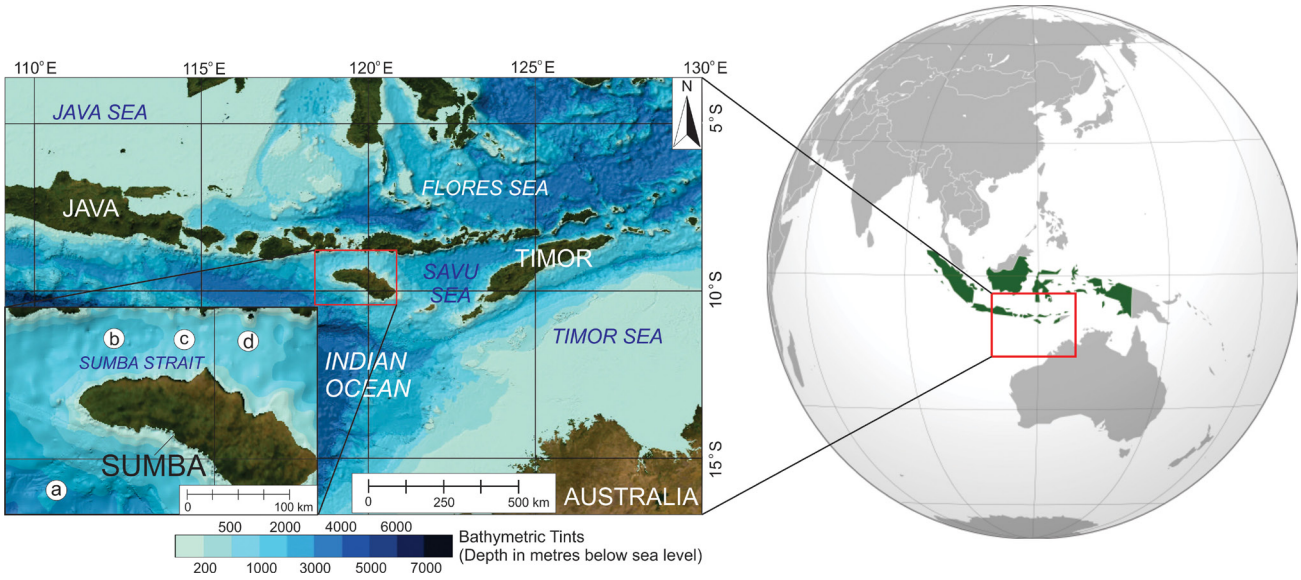

Figure 1: Locations of gravity cores collection on the southwest Sumba offshore and Sumba Strait: ST08 (a), ST14 (b), ST13 (c), and ST12 (d). Bathymetric data were obtained from **GEBCO Bathymetric Compilation Group 2020 (2020)**.

of ITF (**Kuhnt et al., 2004; Spooner et al., 2005; Holbourn et al., 2011; Ding et al., 2013**). During the Last Glacial–Deglaciation, the DOT became shallower due to the perpetual occurrence of AIWM in southern Indonesia, except in the main ITF outflow region (the Timor Sea), while the paleoproductivity in this region was generally higher (**Kuhnt et al., 2004; Holbourn et al., 2005, 2011; Xu et al., 2006; Ding et al., 2013**). In the Java upwelling region, the increased paleoproductivity was caused by the enhanced coastal upwelling (**Andruleit et al., 2008; Lückge et al., 2009; Mohtadi et al., 2011a**). The enhanced paleoproductivity in the Timor Sea was associated with the exposure of Sahul Shelf which enhanced the nutrient supply to the ocean (**Kuhnt et al., 2004; Kawamura et al., 2006; Capelli et al., 2016**) and the hydrographic change of ITF's water mass related to the slowdown of thermohaline circulation during the Last Glacial–Deglaciation (**Martínez et al., 1999; Xu et al., 2006**). During the Holocene, the paleoproductivity was generally lower and the DOT shoaling was only indicated in the Timor Sea (**Kuhnt et al., 2004; Holbourn et al., 2005, 2011; Xu et al., 2006**). The lower paleoproductivity was related to the weakened coastal upwelling and the submerged Sahul Shelf (**Holbourn et al., 2005; Kawamura et al., 2006; Capelli et al., 2016**).

The Sumba Island offshore is situated at the confluence of the ITF's exit passage and the Java upwelling region. The mechanism for the past DOT and paleoproductivity changes is still not well understood in this region, as most of the previous studies focused on the main ITF exit passage (Timor Sea) (**Müller and Opdyke, 2000; Kuhnt et al., 2004; Holbourn et al., 2005, 2011; Xu et al., 2006, 2008; Xu, 2014**), and similar studies on minor paths (i.e. Ombai Strait and Sumba Strait) are still scarce (**Steinke et al., 2014b; Ardi et al., 2019; Putra and Nugroho, 2020**). This preliminary research aimed to reveal the mechanism of paleoproductivity changes at the Sumba Island offshore, were they accompanied by the DOT changes? In this research, the DOT and paleoproductivity changes were inferred from foraminiferal assemblages of three marine sediment (gravity) cores taken from Sumba Strait (ST12, ST13, and ST14) and a gravity core taken from southwest Sumba offshore (ST08) (see **Figure 1**).

2. Climate and Oceanographic Setting

The oceanography of the Indonesian seas is highly influenced by the AIM and ITF **(Gordon, 2005; Ding et al., 2013; Sprintall and Révelard, 2014**). The semi-annual latitudinal shifts of the Inter-tropical Convergence Zone (ITCZ) result in the contrast climate condition between Australian-Indonesian summer monsoon (AISM) (December–March) and AIWM (April–September) (**Mohtadi et al., 2016; Wang et al., 2017**). The peak of AISM coincides with the southern hemisphere/austral summer when the ITCZ lies around the latitude of Northern Australia, while the AIWM reaches its peak during the northern hemisphere/boreal summer when the ITCZ lies around the latitude of Indochina (**Wheeler and McBride, 2005; Yim et al., 2014; Huang et al., 2015**) (see **Figure 2**). During the AISM, the northwest winds bring the moisture-rich air to the Indonesia region and induce the wet season, while the drier southeast winds during AIWM deliver the dry season (**Wheeler and McBride, 2005**). The rainfall difference between the wet and dry seasons in the Indonesian region is most prominent in its southern part (from Southern Sumatra to the Lesser Sunda Islands) which indicates the stronger monsoon influence (**Aldrian and Susanto, 2003; Mohtadi et al., 2007**).

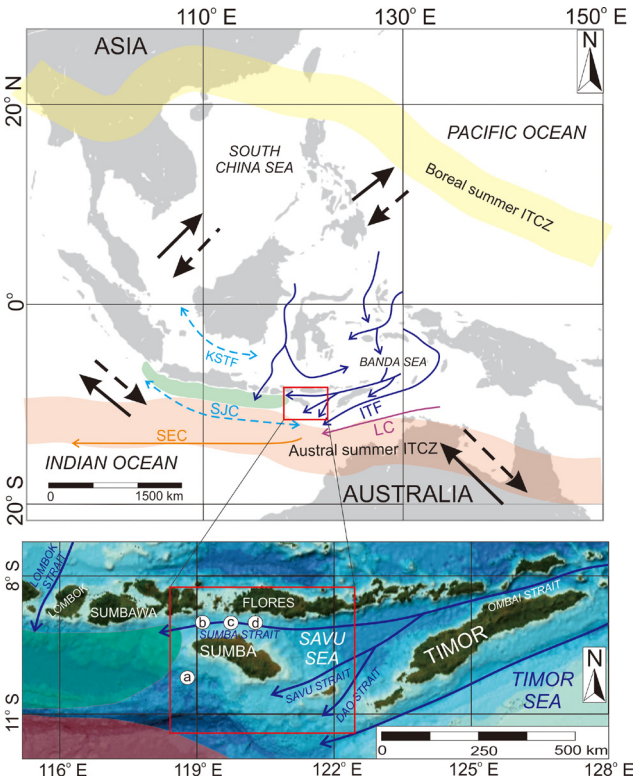

Figure 2: Modern climate and oceanography of Indonesia adapted from several authors (**Gordon, 2005; Qu et al., 2005; Andruleit et al., 2008; Sprintall et al., 2009; Ningsih et al., 2013; Kuhnt et al., 2015; Wang et al., 2017; Bayhaqi et al., 2019**). Red-outlined rectangular indicates the study area, white circles indicate the location of the studied cores (a. ST08, b. ST14, c. ST13, and d. ST12), blue arrows indicate ITF routes, cyan dashed arrows indicate the seasonally reversed currents (SJC and KSTF), the purple arrow indicates LC, orange arrow indicates SEC, green shading indicates the Java upwelling region, yellow shading indicates the Boreal summer ITCZ and red shading indicates the Austral summer ITCZ. Bathymetric data were obtained from **GEBCO Bathymetric Compilation Group 2020 (2020)**.

During AISM, the northwest winds bring the warm and relatively fresh surface waters from the South China Sea, Karimata Strait, and the Java Sea to the southern tip of Makassar Strait and the Flores Sea in the form of Karimata Strait Through-flow (KSTF) (**Tomczak and Godfrey, 2003; Qu et al., 2005**) (see **Figure 2**). This water mass blocks the ITF surface water and causes the formation of thermocline-dominated ITF, which in turn causes shoaling of the DOT in the ITF exit passage (**Gordon et al., 2003; Qu et al., 2005**). The northwest winds also affect the direction of another surface current, i.e. South Java Current (SJC), which flows to the southeast, bringing the water mass from the equatorial Indian Ocean to the Timor Sea before merging with the Leeuwin Current (LC), and the water mass from ITF to form the South Equatorial Current (SEC) (**Schott and McCreary, 2001; Tomczak and Godfrey, 2003; Spooner et al., 2005**) (see **Figure 2**). During AIWM, the southeast winds cause the KSTF and SJC to flow in the opposite direction (to the northwest) **(Schott and McCreary, 2001; Tomczak and Godfrey, 2003; Qu et al., 2005**). The northwest flow of KSTF dismisses the surface water barrier in the southern tip of Makassar Strait, thus allows the ITF surface water to enter the Flores Sea, causing the DOT shoaling in the ITF exit passage (**Gordon et al., 2003; Qu et al., 2005**). The occurrence of ITF's surface and thermocline water indicates that the intensity of ITF is relatively higher and reaches its maximum around August (**Tomczak and Godfrey, 2003**). The northwest flow of KSTF draws surface water masses from the Flores and Banda Sea, which triggers the minor upwelling in the Banda Sea (**Spooner et al., 2005; Brijker et al., 2007**). During this time, the SJC flows northwest and brings the water mass from the ITF exit passage to the equatorial Indian Ocean **(Schott and McCreary, 2001; Tomczak and Godfrey, 2003**). The northwest flow of SJC triggers the seasonal coastal upwelling in the Java upwelling region, which reaches its maximum around August **(Susanto et al., 2001; Ningsih et al., 2013**).

Most of the ITF water mass (~15 Sv) enters the Indian Ocean through its main exit passage, which is the Timor Sea (~7.5 Sv), while some of it passes through the Lombok Strait (~2.6 Sv) and Ombai Strait (~4.9 Sv) (**Sprintall et al., 2009**). The ITF water mass that flows through the Ombai Strait enters the Savu Sea before diverging to the Sumba Strait and the Savu/Dao Straits (**Potemra et al., 2003; Sprintall et al., 2009**). A recent study by **Bayhaqi et al. (2019**) revealed very small transport of ITF (~0.1 Sv) that flows through the Sumba Strait compared to the Savu/Dao Straits.

On an interannual scale, the oceanography of the Indonesian region is influenced by the *El Niño* Southern Oscillation (ENSO) and Indian Ocean Dipole (IOD), especially the upwelling intensity (**Ningsih et al., 2013; Chen et al., 2016; Kusuma et al., 2017; Hendrawan et al., 2019**). The occurrence of *El Niño* (*La Niña*) and positive (negative) IOD phases is associated with the more (less) intense coastal upwelling due to the anomalous stronger southeast (northwest) winds (**Susanto et al., 2001; Sprintall et al., 2003; Ningsih et al., 2013**). ENSO-like and IOD-like mechanisms, which are defined as the occurrence of several periods with more frequent *El Niño*/*La Niña*/positive IOD/negative IOD phase at millennial – multi-millennial scale, are also inferred in the Indonesia region (**Brijker et al., 2007; Abram et al., 2009; Kwiatkowski et al., 2015; Feng et al., 2018**).

3. Material and Methods

Four gravity cores collected during the 2016 Widya Nusantara Expedition (E-WIN) from off southwest Sumba (ST08) and from Sumba Strait (ST12, ST13, and ST14) were used as the research materials (see **Table 1**). The samples for foraminifera determination and count-

Table 1: Gravity cores used in this study

Core	Location	Coordinate		Depth (metres below sea level)	Length (cm)
		Longitude (°E)	Latitude (°S)		
ST08	Off southwest Sumba	118.772	10.195	2966	236
ST12	Sumba Strait	120.243	9.068	830	223
ST13	Sumba Strait	119.740	9.072	1004	173
ST14	Sumba Strait	119.245	9.079	1283	243

Table 2: AMS ^{14}C ages and calibrated ^{14}C ages of core ST08 (**Ardi, 2018**)

Lab Code	Depth Intervals	Materials	^{14}C age (BP)	Calibrated ^{14}C age BP
Beta-492272	24–25 cm	Foraminifera : *Neogloboquadrina* spp.	3330 ± 30	3236–2938
Beta-492271	74–75 cm	Foraminifera : *Neogloboquadrina* spp.	4880 ± 30	5272–4948
Beta-492270	104–105 cm	Foraminifera : *Neogloboquadrina* spp.	6390 ± 30	6920–6660
Beta-449813	166–167 cm	Bulk Sediment	11930 ± 30	13430–13330 (13375)
Beta-449814	235–236 cm	Bulk Sediment	15510 ± 50	18480–18255 (18360)

ing were taken following the sampling procedure of **Ardi** (**2018**), **Ardi et al.** (**2019**), **Damanik et al.** (**2019**), and **Putra and Nugroho** (**2020**). A total of 250 sub-samples were collected and ~5 g from each sub-sample were prepared using the swirling method (without H_2O_2) to disengage the foraminifera specimens from the mud. Each sample was washed on the top of 200 mesh (0.074 mm) sieve and the residue was dried at the temperature of 60°C for ~6 hours.

Quantitative determination of foraminiferal taxa was preceded by splitting the prepared sample until ~300 specimens of foraminifera were present in each part. All identified taxa in one part were counted while new taxa detected in the remaining parts were counted as one specimen even after normalization. The foraminiferal counts were normalized against the number of splits and the weight of the samples (**Ardi et al., 2019**). Planktonic foraminifera descriptions by **Kenneth and Srinivasan** (**1983**) and **Bolli and Saunders** (**1985**) were referred. The sample preparations and the determination and counting of foraminifera were conducted at the Sedimentary Laboratory of the Research Center for Geotechnology of the Indonesian Institute of Science (LIPI) and the Micropaleontology Laboratory of Institut Teknologi Bandung (ITB).

Accelerator Mass Spectrometer-measured radiocarbon (AMS ^{14}C) ages were only available on five depth intervals of core ST08 (see **Table 2**) (**Ardi, 2018**). The radiocarbon ages were converted to calibrated calendar and radiocarbon ages with High Probability Density Range (HPD) Method (**Bronk Ramsey, 2009**) (for 24–25 cm, 74–75 cm, and 104–105 cm depth intervals), and the intercept of radiocarbon age with calibration curve (**Talma and Vogel, 1993**) (for 166–167 cm and 235–236 cm depth intervals) based on the MARINE13 calibration datasets (**Reimer et al., 2013**). The age model for the core ST08 was generated using the Clam package (version 2.3.4) on R (**Blaauw, 2010, 2020; R Core Team, 2013**). This standard statistic approach is the better choice to rapidly and systematically produce age-models for the low-resolution dating sites since the use of complicated Bayesian age-modeling methods might not add much accuracy and precision (**Blaauw, 2010**). Twenty runs were done, and a model with the lowest goodness-of-fit (-log) was chosen. This model employed linear interpolation, weighted average-based calendar age point estimates for depths, and the standard Gaussian distribution. The core top sediment was assumed to be aged -66 Before Present (BP) (Present=1950 Anno Domini/AD, core ST08 was retrieved in 2016) and the sedimentation rates between the aged intervals were assumed to be constant (see **Figure 3** and **Table 3**). The sedimentation rates abruptly increased in 25–74 and 75–104 cm depth intervals which were coeval to Mid Holocene, while the sedimentation rates of 0–24 cm, 105–166 cm, and 167–236 cm depth intervals (coeval to Late Holocene, Late Deglaciation–Early Holocene, and Early Deglaciation) were relatively lower (see **Figure 3**). Relative age based on planktonic foraminiferal zonation (**Bolli and Saunders, 1985**) was also utilized to establish the chronological framework in this study. Pleistocene-aged sediments were only inferred on core ST08, ST13, and ST14 while Holocene-aged sediments were inferred on all cores, including core ST12.

The relative abundances of thermocline dwellers (i.e. *Pulleniatina obliqueloculata*, *Neogloboquadrina* spp. and *Globorotalia* spp.) and mixed layer dwellers (i.e. *Globigerinoides ruber*, *Globigerinoides trilobus*, and other *Globigerinoides* taxa) planktonic foraminifera (ratio of the total number of thermocline/mixed layer dwellers against the total number of planktonic foraminifera in a subsample) (see Supplementary Materials**)** were used to infer the changes in the DOT, as suggested by **Bé et al. (1977**) and **Ravelo et al.** (**1990**). The shoaling (deepening) of the DOT was indicated by the increase

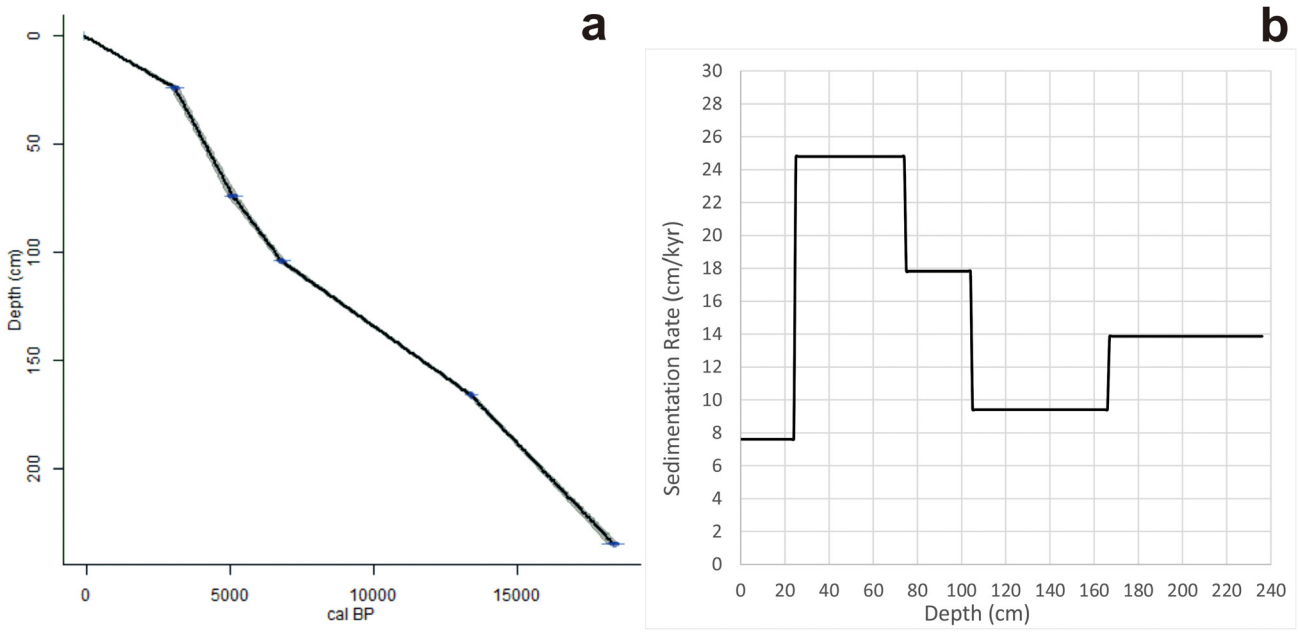

Figure 3: Age model based on the standard statistic approach using the Clam package on R (**Blaauw, 2010, 2020; R Core Team, 2013**). The best-estimated ages are hinted by the bold line (a). Sedimentation rates between the aged depth intervals (b).

Table 3: Sedimentation rates used in the age model, obtained from the Clam package on R (**Blaauw, 2010, 2020; R Core Team, 2013**).

Depth intervals	Sedimentation rates (cm/ka)
0–25 cm	7.602
25–75 cm	24.802
75–105 cm	17.825
105–167 cm	9.407
167–236 cm	13.864

(decrease) of the thermocline (mix layer) dwellers' abundance (**Ravelo et al., 1990; Spooner et al., 2005; Maryunani, 2009; Ding et al., 2013; Steinke et al., 2014b**). The relative abundance of *Neogloboquadrina* (*N.*) *dutertrei* (ratio of the *N. dutertrei* against the total number of planktonic foraminifera in a subsample) (see Supplementary Materials**)**, a typical taxon that prefers to live in a high productivity condition around the Deep Chlorophyll Maximum (DCM) layer, was used to infer the paleoproductivity (**Barmawidjaja et al., 1993; Spooner et al., 2005; Mohtadi et al., 2007; Zhang et al., 2016, 2019**).

4. Results and Discussion

The proxies used in this study (thermocline dwellers, mixed layer dwellers, and *N. dutertrei*) exhibit changes within the Holocene and Pleistocene (Last Deglaciation) periods. Spatial differences of thermocline dwellers, mix layer dwellers, and *N. dutertrei* changes are also observed in the research area.

4.1 Core ST08 (off southwest Sumba)

Based on the age model of core ST08 (see **Figure 3**), the first occurrence (FO) of *Globorotalia* (*Gl.*) *fimbriata* which indicates the beginning of the Holocene is coeval to ~11 ka BP (see **Figure 4**). The abrupt changes in thermocline dwellers, shallow dwellers, and *N. dutertrei* were observed around this time, which indicated a contrast abundance pattern during the Last Deglaciation, and the Holocene. Thermocline dwellers and *N. dutertrei* were significantly higher during the Last Deglaciation and significantly lower during the Holocene, however, less notable changes were also observed within the Last Deglaciation and Holocene intervals (see **Figures 5** and **6**). Less notable increases of thermocline dwellers were indicated around Mid Holocene (80–120 cm and 60–65 cm intervals) and Late Holocene (0–20 cm interval) (see **Figure 5**). *N. dutertrei* was slightly increased around Mid Holocene (80–120 cm interval) and slightly decreased around Mid Deglaciation (180–200 cm interval) (see **Figure 6**). Mixed layer dwellers showed a contradictive pattern compared to the thermocline dwellers and *N. dutertrei* with lower abundance during the Last Deglaciation and higher abundance during the Holocene (see **Figure 7**). During the Holocene, minor decreases are detected around Mid Holocene (90–115 cm and 60–65 cm intervals) and Late Holocene (0–20 cm interval).

The higher abundance of thermocline dwellers and the lower abundance of mixed layer dwellers indicated a shallower DOT during the Last Deglaciation compared to the Holocene (see **Figures 5** and **7**). Minor increases of the thermocline dwellers and minor decreases of the mixed layer dwellers around the Mid and Late Holocene

also indicated DOT shoaling but to a lesser extent. Paleoproductivity was higher during the Last Deglaciation and lower during the Holocene (see **Figure 6**). A minor decrease of paleoproductivity was indicated around the Mid Deglaciation while its minor increase occurred around the Mid Holocene (see **Figure 6**).

4.2 Core ST14 (western Sumba Strait)

The pattern of the thermocline and mixed layer dwellers were similar to the core ST08 but with a less obvious shift (see **Figures 5** and **7**). The shift of the thermocline and mixed layer dwellers occurred earlier compared to the core ST08, which was around the Late Deglaciation (~170–180 cm interval) (see **Figures 5** and **7**). A minor increase of thermocline dwellers and a minor decrease of mixed layer dwellers were also observed around the Late Holocene (0–30 cm interval). The abundance of *N. dutertrei* was more constant with a more obvious increase observed around the Mid Deglaciation (150–170 cm interval) and a less significant increase around the Mid Holocene (40–60 cm interval) (see **Figure 6**).

A shallower DOT was indicated during the Last Deglaciation, but a deepening of the DOT occurred earlier compared to the southwest Sumba offshore (around the Late Deglaciation). In addition, the shoaling of the DOT around the Mid Holocene was not detected (see **Figures 5** and **7**). Minor DOT shoaling was also indicated around the Late Holocene, as the abundance of thermocline dwellers was gradually increased, and the abundance of mixed layer dwellers decreased gradually. Paleoproductivity was mostly constant with a more significant increase around the Mid Deglaciation and a less significant increase around the Mid Holocene (see **Figure 6**).

4.3 Core ST13 (central Sumba Strait)

The pattern of the thermocline dwellers and *N. dutertrei* was relatively constant around the Last Deglaciation–Early Holocene (90 cm–bottom interval) and gradually increased afterward (0–90 cm interval) (see **Figure 5** and **6**). Mixed layer dwellers were less abundant during the Last Deglaciation until the earliest interval of Holocene (140 cm–bottom interval), before increasing around the Early Holocene (80–140 cm interval), and decreased gradually since the Mid Holocene (see **Figure 7**).

The DOT was relatively constant during the Late Deglaciation–Early Holocene before it gradually shoaled since the Mid Holocene (see **Figures 5** and **7**). Paleoproductivity also indicated a similar pattern which gradually increased since the Mid Holocene (see **Figure 6**).

4.4 Core ST12 (eastern Sumba Strait)

Core ST12 only recorded Holocene-aged sediments, indicated by the occurrence of *Gl. fimbriata* even in its lowest interval. The abundance of thermocline dwellers was slightly lower around the Early Holocene (100 cm–bottom interval) compared to around Late Holocene (0–80 cm interval) while a significant decrease was observed around the Mid Holocene (80–110 cm interval) and a minor decrease was observed around the Late Holocene (0–20 cm interval) (see **Figure 5**). The abundance pattern of mixed layer dwellers mirrors the thermocline dwellers with a significant increase around Mid Holocene (80–110 cm interval) and a minor increase around the Late Holocene (0–20 cm interval) (see **Figure 7**). A significant decrease of *N. dutertrei* was indicated around the Mid Holocene (70–140 cm interval) while the higher abundance of *N. dutertrei* was observed around the Early Holocene (140 cm–bottom interval) and around the Late Holocene (0–70 cm interval) (see **Figure 6**).

During the Holocene, the shoaling of DOT occurred twice on the eastern Sumba Strait. The more significant DOT shoaling occurred around Mid Holocene, while the less significant DOT shoaling occurred around Late Holocene (see **Figures 5** and **7**). A paleoproductivity decrease was indicated around the Mid Holocene, while around the Late Holocene, it was increased (see **Figure 6**).

4.5 The mechanism of DOT and paleoproductivity changes

Based on the analyzed proxies, the DOT at the Sumba Island offshore (southwest Sumba offshore and Sumba Strait) got shallower during the Last Deglaciation and deeper during the Holocene, as it was opposed to the DOT at the Timor Sea, the main exit passage of ITF (**Xu et al., 2008; Holbourn et al., 2011; Kuhnt et al., 2015**). This indicated that the glacial-interglacial hydrographic changes of ITF were not the main driver for the past DOT changes, but the multi-millennial changes of the AIM. DOT and paleoproductivity changes within the Holocene and Last Deglaciation periods are also inferred.

DOT shoaling at the Last Deglaciation was caused by the enhancement of coastal upwelling due to the stronger AIWM during this period (**Spooner et al., 2005; Mohtadi et al., 2011a; Ding et al., 2013**). Stronger AIWM during the Last Deglaciation was associated with the northward shift of the Austral summer ITCZ to around the latitude of Flores Island (Figure 8) hence the AISM northwest winds couldn't reach the Sumba Island offshore (**Spooner et al., 2005; Xu et al., 2006; Ding et al., 2013; Kuhnt et al., 2015; Ishiwa et al., 2019**). The enhanced coastal upwelling during this period resulted in the eutrophic condition indicated by higher paleoproductivity in the southern Indonesia region (**Ding et al., 2013; Xu, 2014**), including the Sumba Island offshore. A slight decrease of paleoproductivity around Mid Deglaciation (see **Figure 6**) was most likely not related to the upwelling intensity, as the DOT remained constant. The change of the lifted water mass characteristics was suggested as the cause for the paleoproductivity reduction. The lifted water mass was most likely the North

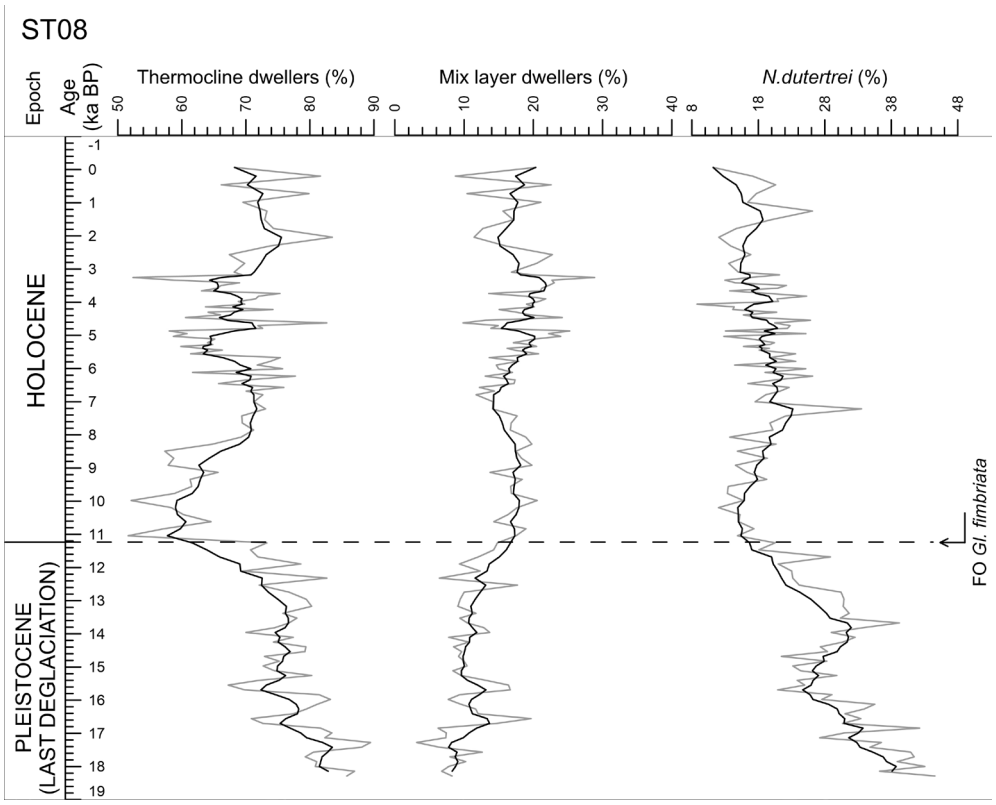

Figure 4: Plot of thermocline dwellers, mixed layer dwellers, and *N. dutertrei* abundances (%) of core ST08 based on the age model. The dashed line indicates the FO of *Gl. fimbriata* (Pleistocene–Holocene boundary).

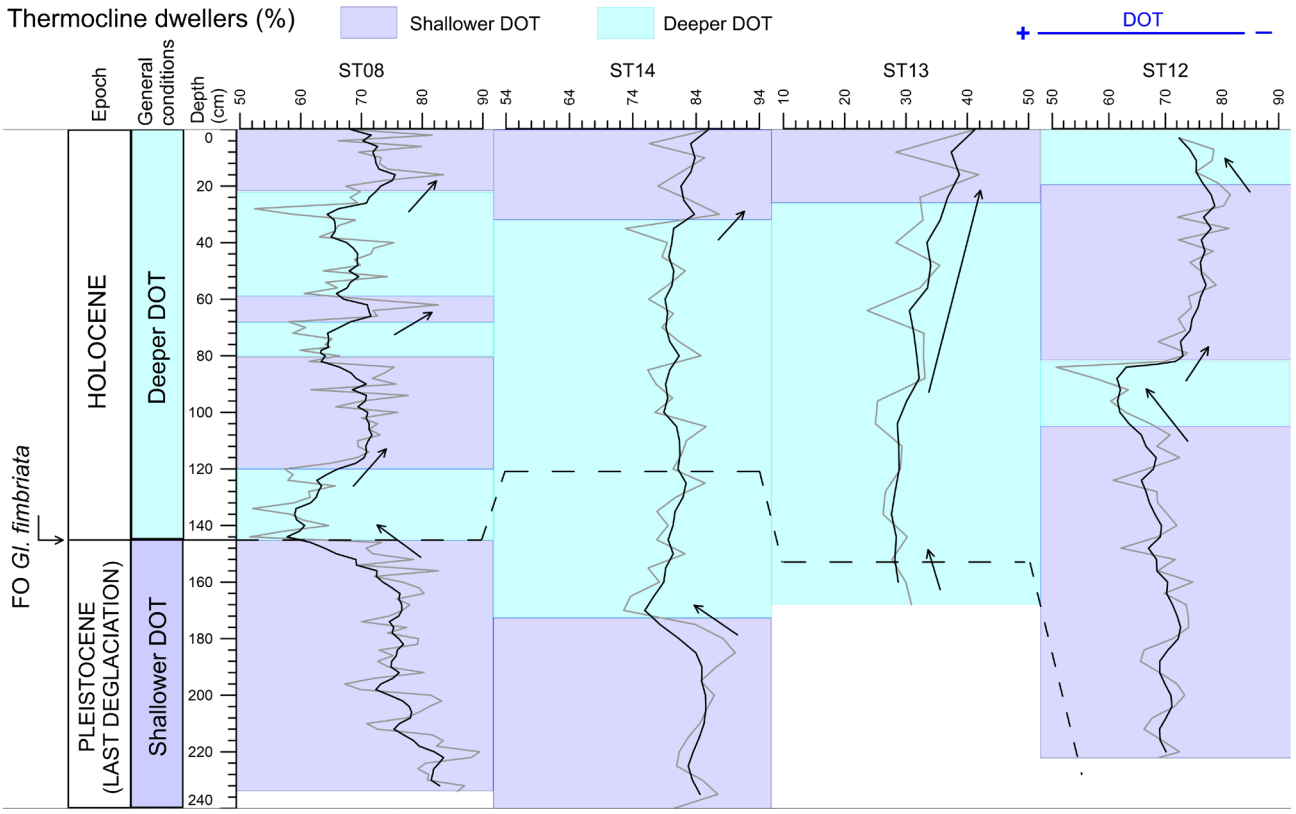

Figure 5: Thermocline dwellers abundances (%) of core ST08, ST14, ST13, and ST12 against depth. The dashed line indicates the FO of *Gl. fimbriata* (Pleistocene–Holocene boundary).

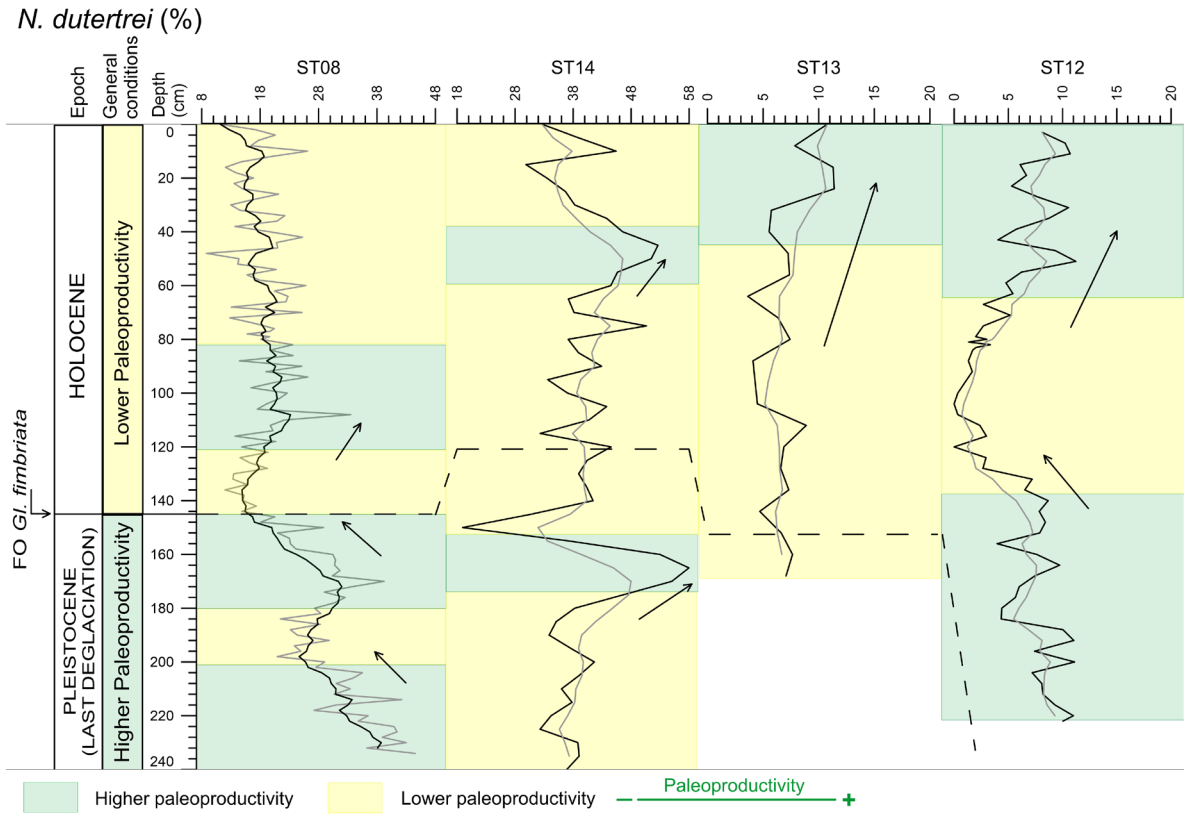

Figure 6: *N. dutertrei* abundances (%) of core ST08, ST14, ST13, and ST12. The dashed line indicates the FO of *Gl. fimbriata* (Pleistocene–Holocene boundary).

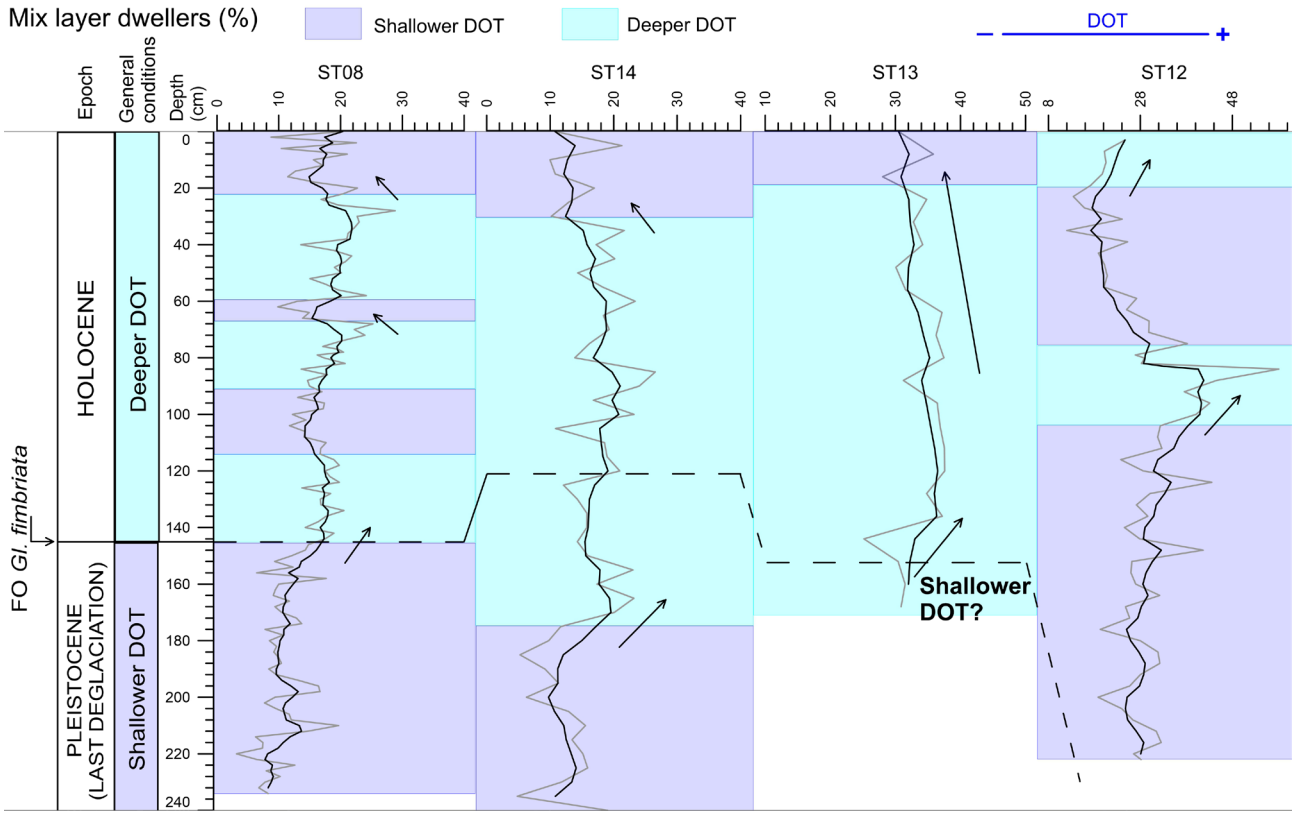

Figure 7: Mixed layer dwellers abundances (%)of core ST08, ST14, ST13, and ST12 against depth. The dashed line indicates the FO of *Gl. fimbriata* (Pleistocene–Holocene boundary).

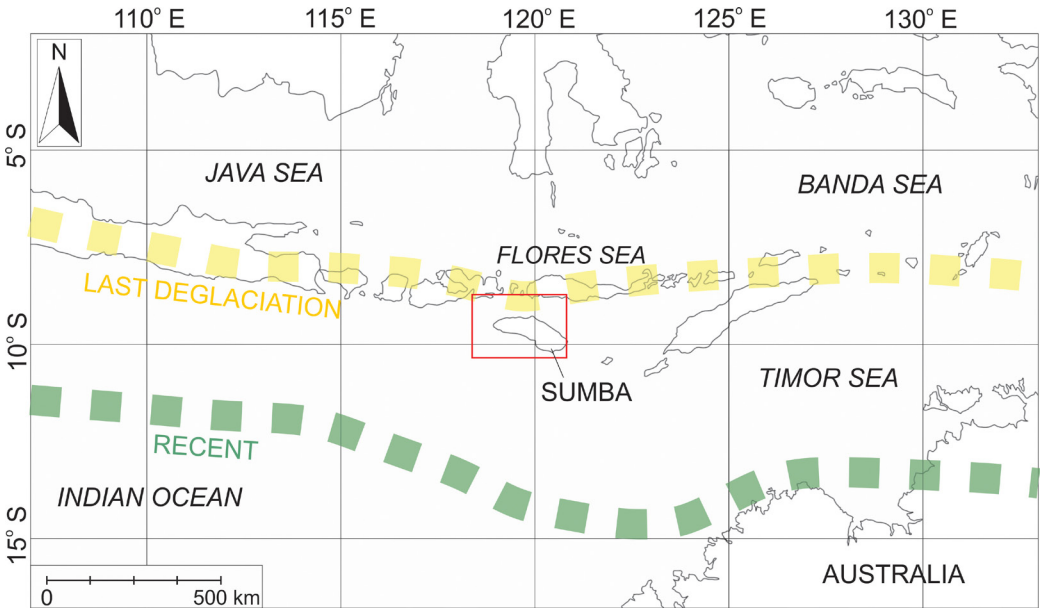

Figure 8: The southern limit of Austral summer ITCZ: present-day condition (the green dashed line) and tentative position during the Last Deglaciation (yellow dashed lines) (**Kuhnt et al., 2015; Ardi et al., 2020**). The red-lined rectangular indicates the study area.

Pacific Intermediate Water (NPIW) which entered the sea off Sumba Island as a part of the ITF (**Bayhaqi et al., 2019**). The changes in the characteristics of ITF water mass were related to the strengthening (weakening) of Atlantic Meridional Ocean Circulation (AMOC) during the Last Deglaciation warm (cold) periods which accelerated (stalled) the thermohaline circulation (**Kuhnt et al., 2004; Xu et al., 2006; Levi et al., 2007; Deplazes et al., 2013; Gibbons et al., 2014; Lynch-Stieglitz et al., 2014**). The freshening and the warming of the thermohaline circulation water mass due to the melting of the North Atlantic ice sheets during the Last Deglaciation warm periods most likely resulted in a more nutrient-depleted water mass, and thus, a reduction in the paleoproductivity (**Deplazes et al., 2013; Lynch-Stieglitz et al., 2014; Hendrizan et al., 2017**).

The earlier DOT deepening and paleoproductivity reduction (around the Late Deglaciation) in the Sumba Strait (cores ST12, ST13, and ST14) might be related to its northward position compared to the southwest Sumba offshore (core ST08), thus the AISM reactivated earlier as the Austral summer ITCZ gradually shifted southward (**Wyrwoll and Miller, 2001; Kuhnt et al., 2015**). Despite the lower abundance of mixed-layer dwellers on the central Sumba Strait around the Late Deglaciation, DOT shoaling did not occur due to the relatively lower abundance of thermocline dwellers. Thermocline dwellers consist of the dissolution-resistant taxa (**Ravelo et al., 1990; Martínez et al., 1999**), thus their relative abundance changes are more robust as a proxy for the DOT. In southwest Sumba offshore, which is located southward, the AISM reactivation most likely occurred around the Last Deglaciation–Holocene transition. The lower interval of ST14 (170 cm–bottom interval) (western Sumba Strait), which indicated lower paleoproductivity, is most likely coeval to the 180–200 cm interval of ST08 (southwest Sumba offshore). This indicated that the Early Deglaciation sediment records were only available in the southwest Sumba offshore (ST08) core.

Around the Mid Holocene, DOT shoaling accompanied by higher paleoproductivity (eutrophic condition) only occurred at southwest Sumba offshore. The shoaling of DOT and eutrophic condition was most likely caused by the stronger AIWM (**Steinke et al., 2014b; Ardi et al., 2020**) which enhanced the coastal upwelling, similar to the DOT shoaling mechanism during the Last Deglaciation (**Spooner et al., 2005; Ding et al., 2013**). The stronger AIWM was most likely related to decreasing solar activity (**Solanki et al., 2004; Steinke et al., 2014a**). Increasing austral summer insolation during this period should strengthen the AISM, but its effect was suppressed by the decreasing solar activity **(Steinke et al., 2014a; Ardi et al., 2020**). In the Sumba Strait, a change of the DOT was only indicated in its eastern part, which was DOT deepening. The deepening of DOT could be related to the intensification of surface water ITF owing to stronger AIWM (**Ding et al., 2013**). The intense AIWM would transfer the more saline Banda Sea waters to the southern tip of the Makassar Strait, thus displaced the freshwater plug that blocked the surface water ITF (**Xu et al., 2006; Ding et al., 2013**). The deepening of the DOT indicated that the effect of ITF variability could reach the Sumba Strait, even though this was only in its eastern part. The deepening of the DOT also resulted in the lower paleoproductivity (oligotrophic) condition at eastern Sumba Strait, as a thicker mix layer would inhibit the eutrophication process (**Brasier, 1995**) and vertical mixing was not effective

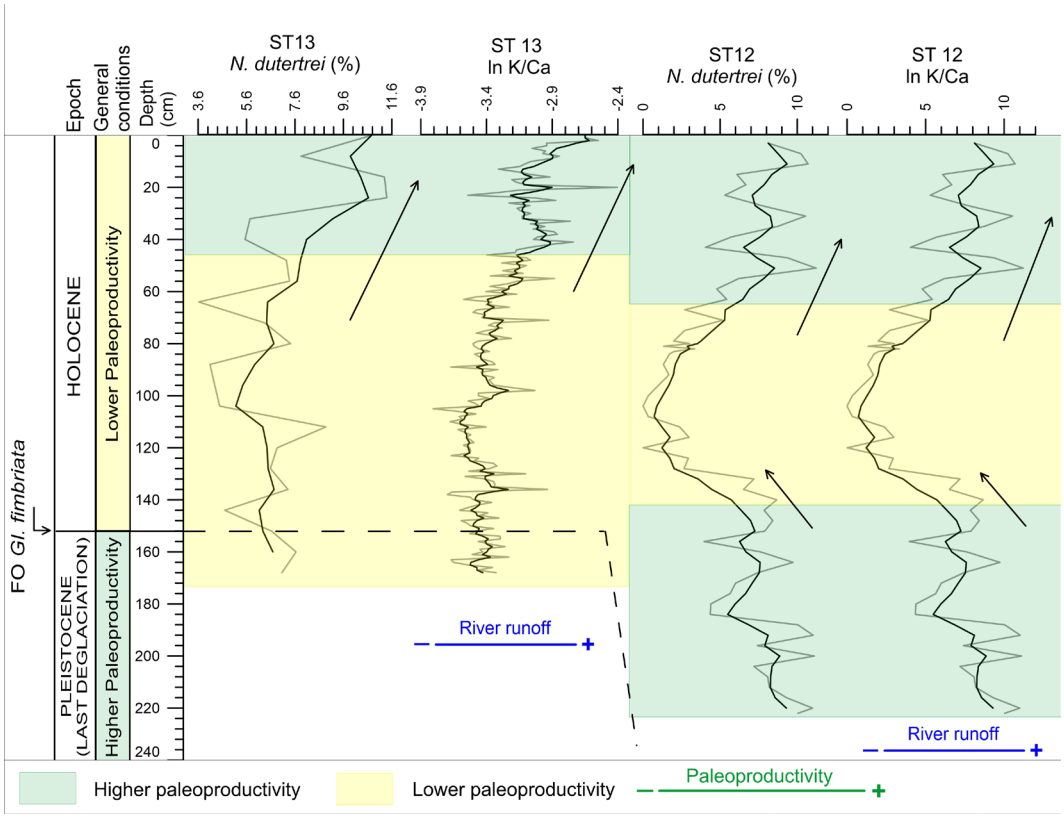

Figure 9: Plot of *N. dutertrei* abundances compared to riverine input proxy (ln K/Ca) in central and eastern parts of Sumba Strait (core ST13 and ST12). The dashed line indicates the FO of *Gl. fimbriata* (Pleistocene–Holocene boundary).

due to the narrow size of Sumba Strait (**Bayhaqi et al., 2019**). In central and western Sumba Strait, the effect of ITF variability was most likely counteracted by the AIWM-induced oceanographic changes, as indicated by the paleoproductivity enhancement in western Sumba Strait.

Late Holocene DOT shoaling was observed at southwestern Sumba offshore, western and central Sumba Strait while the eutrophic condition was only indicated in the central and eastern Sumba Strait. Late Holocene ENSO intensification which resulted in an *El Niño*-like condition (**Brijker et al., 2007; Wanner et al., 2008; Chen et al., 2016**) was most likely the cause for the DOT shoaling, along with the positive IOD-like condition (**Abram et al., 2009; Kwiatkowski et al., 2015**). Present *El Niño* and positive IOD years are associated with the anomalously strong southeast winds during AIWM which enhanced the coastal upwelling (**Susanto et al., 2006; Ningsih et al., 2013**). The relatively constant paleoproductivity at the southwest Sumba offshore and western Sumba Strait could be related to the lesser scale of upwelling enhancement compared to around the Mid Holocene and the Last Deglaciation. Despite the *El Niño*-like and positive IOD-like condition, which should have resulted in an enhanced AIWM condition, AISM was stronger, thus increasing the rainfall during this period (**Steinke et al., 2014a; Ardi et al., 2020**). Higher rainfall enhanced the river runoff, which most likely caused the increase of nutrient availability in the surface water (**Kawamura et al., 2006; Steinke et al., 2014a**). This mechanism explains the eutrophic conditions inferred in the central and eastern Sumba Strait which coincided with the enhancement of the riverine input proxy (ln K/Ca) (see **Figure 9**). This mechanism was more effective in the central and eastern Sumba Strait due to its proximity to the surrounding islands compared to the southwest Sumba offshore and the western Sumba Strait. A similar mechanism was also indicated off southwest Java during the Late Holocene, which resulted in the higher paleoproductivity condition **(Setiawan et al., 2015; Xu et al., 2017**). The eutrophic condition in central and eastern Sumba Strait also indicates the direct relationship of *N. dutertrei* with the freshwater influx caused by the increase of river runoff due to AISM enhancement (**Mohtadi et al., 2011b; Steinke et al., 2014a**), especially in a geographically-restricted sea. The cause of the DOT deepening in the eastern Sumba Strait was most likely identical to the DOT deepening that occurred around the Mid Holocene while the intensification of surface water ITF was related to the *El Niño*-like condition (**Hendrizan et al., 2017**).

The use of the relative abundance of planktonic foraminifera as a proxy to interpret the DOT and paleoproductivity has been proven effective in the southern Indo-

nesia region (**Spooner et al., 2005; Ding et al., 2013; Steinke et al., 2014b; Ardi, 2018; Ardi et al., 2019**). Despite the effectiveness, the interpreted DOT and paleoproductivity from the relative abundance of planktonic foraminifera were basically qualitative. The use of geochemical proxies from both the foraminifera tests ($\delta^{18}O$, $\delta^{13}C$, Mg/Ca, etc.) and bulk sediments (total organic carbon, carbonate content, etc.) is suggested to produce more plausible results in future studies. In addition, radiocarbon dating data of the Sumba Strait cores (ST12, ST13, and ST14) is needed to produce more robust geochronology and simplify the proxies comparison between the studied cores.

5. Conclusions

(1) DOT:

A contrast DOT pattern compared to the Timor Sea (main exit passage of ITF) during the Last Deglaciation–Holocene was indicated at the Sumba Island offshore based on thermocline and mixed layer dwellers' relative abundances. This concluded that the glacial-interglacial hydrographic changes of ITF did not cause the DOT changes at Sumba Island offshore, instead, they were primarily driven by the AIM variability. The role of ENSO-like and IOD-like mechanisms to the DOT changes was only indicated around the Late Holocene. The effect of ITF changes might reach the eastern Sumba Strait, which was indicated by the shallower DOT around the Mid and Late Holocene.

(2) Paleoproductivity:

N. dutertrei relative abundance indicated that the monsoon-driven coastal upwelling intensification which resulted in DOT shoaling and eutrophic condition was not always the cause for the paleoproductivity enhancement. The increase of nutrient availability in surface water due to the increase of river runoff and the changes in the lifted water mass nature were also able to enhance paleoproductivity.

6. Acknowledgement

This research is part of the concept of sustainable coastal environmental management for eutrophication disaster mitigation research in the Priority Research and Demand Drive Research Coremap-CTI (Number: SP DIPA- 079.01.1.664156/2020). We express our gratitude to Dr. Dyah Marganingrum for the permission to participate in this research. We also thank the Research Center for Oceanography of LIPI, especially Udhi Hermawan, Ph.D. as the chief scientist of E-WIN 2016 for the permission of data usage and administrative assistance and all crews of the Baruna Jaya VIII R.V., especially Singgih Adi Wibowo for technical supports and data collecting. The Research Center for Geotechnology of LIPI and Geological Engineering Department of ITB are thanked for the laboratory facilities. We also express our gratitude to the Indonesian Endowment Fund for Education (LPDP) (grant number: 202001110215954) for the financial assistance. Istiana, Adwi Arya, Adrianus Damanik, and Ahmad Nabil are thanked for their assistance in sample preparation and observation for core ST08, ST12, ST13, and ST14. Rizky Amalia Maulidiatsani is thanked for the assistance in proofreading.

7. Abbreviations

AIM: Australian-Indonesian monsoon
AISM: Australian-Indonesian summer monsoon
AIWM: Australian-Indonesian winter monsoon
AMS: Accelerator Mass Spectrometry
DOT: Depth of thermocline
E-WIN: Widya Nusantara Expedition
FO: First occurence
ENSO: *El Niño* Southern Oscillation
HPD: High Probability Density
IOD: Indian Ocean Dipole
ITB: Institut Teknologi Bandung
ITCZ: Inter-tropical Convergence Zone
ITF: Indonesian Through-flow
KSTF: Kalimantan Strait Through-flow
LC: Leeuwin Current
LIPI: Indonesian Institute of Sciences
NPIW: North Pacific Intermediate Water
SEC: South Equatorial Current
SJC: South Java Current

8. References

Papers:

Abram, N. J., McGregor, H. V., Gagan, M. K., Hantoro, W. S., and Suwargadi, B. W. (2009): Oscillations in the southern extent of the Indo-Pacific Warm Pool during the mid-Holocene. Quaternary Science Reviews, 28(25–26), 2794–2803. https://doi.org/10.1016/j.quascirev.2009.07.006

Aldrian, E., and Susanto, R. D. (2003): Identification of three dominant rainfall regions within Indonesia and their relationship to sea surface temperature, International Journal of Climatology, 23(12), 1435–1452. https://doi.org/10.1002/joc.950

Andruleit, H., Lückge, A., Wiedicke, M., and Stäger, S. (2008): Late Quaternary development of the Java upwelling system (eastern Indian Ocean) as revealed by coccolithophores. Marine Micropaleontology, 69(1), 3–15. https://doi.org/10.1016/j.marmicro.2007.11.005

Ardi, R. D. W., Aswan, Maryunani, K. A., Yulianto, E., Putra, P. S., Nugroho, S. H., and Istiana (2020): Last Deglaciation—Holocene Australian-Indonesian Monsoon Rainfall Changes Off Southwest Sumba, Indonesia. Atmosphere, 11(9), 932. https://doi.org/10.3390/atmos11090932

Barmawidjaja, B. M., Rohling, E. J., van der Kaars, W. A., Vergnaud Grazzini, C., and Zachariasse, W. J. (1993): Gla-

cial conditions in the northern Molucca Sea region (Indonesia). Palaeogeography, Palaeoclimatology, Palaeoecology, 101(1–2), 147–167. https://doi.org/10.1016/0031-0182(93)90157-E

Bayhaqi, A., Lenn, Y.-D., Surinati, D., Polton, J., Nur, M., Corvianawatie, C., and Purwandana, A. (2019): The Variability of Indonesian Throughflow in Sumba Strait and Its Linkage to the Climate Events. American Journal of Applied Sciences, 16(4), 118–133. https://doi.org/10.3844/ajassp.2019.118.133

Bé, A. W. H., Hutson, W. H., and Be, A. W. H. (1977): Ecology of Planktonic Foraminifera and Biogeographic Patterns of Life and Fossil Assemblages in the Indian Ocean. Micropaleontology, 23(4), 369. https://doi.org/10.2307/1485406

Blaauw, M. (2010): Methods and code for 'classical' age-modelling of radiocarbon sequences. Quaternary Geochronology, 5(5), 512–518. https://doi.org/10.1016/j.quageo.2010.01.002

Brasier, M. D. (1995): Fossil indicators of nutrient levels. 1: eutrophication and climate change. Marine Palaeoenvironmental Analysis from Fossils, (83), 113–132.

Brijker, J. M., Jung, S. J. A., Ganssen, G. M., Bickert, T., and Kroon, D. (2007): ENSO related decadal scale climate variability from the Indo-Pacific Warm Pool. Earth and Planetary Science Letters, 253(1–2), 67–82. https://doi.org/10.1016/j.epsl.2006.10.017

Bronk Ramsey, C. (2009): Bayesian Analysis of Radiocarbon Dates. Radiocarbon, 51(1), 337–360. https://doi.org/10.1017/s0033822200033865

Capelli, E. L. G., Holbourn, A., Kuhnt, W., and Regenberg, M. (2016): Changes in Timor Strait hydrology and thermocline structure during the past 130 ka. Palaeogeography, Palaeoclimatology, Palaeoecology. https://doi.org/10.1016/j.palaeo.2016.09.010

Chen, G., Han, W., Li, Y., and Wang, D. (2016): Interannual variability of equatorial eastern Indian Ocean upwelling: Local versus remote forcing. Journal of Physical Oceanography, 46(3), 789–807. https://doi.org/10.1175/JPO-D-15-0117.1

Chen, S., Hoffmann, S. S., Lund, D. C., Cobb, K. M., Emile-geay, J., and Adkins, J. F. (2016): A high-resolution speleothem record of western equatorial Pacific rainfall : Implications for Holocene ENSO evolution. Earth and Planetary Science Letters, 442, 61–71. https://doi.org/10.1016/j.epsl.2016.02.050

Deplazes, G., Lückge, A., Peterson, L. C., Timmermann, A., Hamann, Y., Hughen, K. A., Röhl, U., Laj, C., Cane, M. A., Sigman, D. M., and Haug, G. H. (2013): Links between tropical rainfall and North Atlantic climate during the last glacial period. Nature Geoscience, 6(3), 213–217. https://doi.org/10.1038/ngeo1712

Ding, X., Bassinot, F., Guichard, F., and Fang, N. Q. (2013): Indonesian Throughflow and monsoon activity records in the Timor Sea since the last glacial maximum. Marine Micropaleontology, 101, 115–126. https://doi.org/10.1016/j.marmicro.2013.02.003

Feng, M., Zhang, N., Liu, Q., and Wijffels, S. (2018): The Indonesian throughflow, its variability and centennial change. Geoscience Letters, 5(1). https://doi.org/10.1186/s40562-018-0102-2

Gibbons, F. T., Oppo, D. W., Mohtadi, M., Rosenthal, Y., Cheng, J., Liu, Z., and Linsley, B. K. (2014): Deglacial δ18O and hydrologic variability in the tropical Pacific and Indian Oceans. Earth and Planetary Science Letters, 387, 240–251. https://doi.org/10.1016/j.epsl.2013.11.032

Gordon, A. L. (2005): Oceanography of the Indonesian Seas and Their Throughflow. Oceanography, 18(4), 13–13. https://doi.org/10.5670/oceanog.2005.18

Gordon, A. L., and Fine, R. A. (1996): Pathways of water between the Pacific and Indian oceans in the Indonesian seas. Nature. https://doi.org/10.1038/379146a0

Gordon, A. L., Susanto, R. D., and Vranes, K. (2003): Cool Indonesian throughflow as a consequence of restricted surface layer flow. Nature, 425(6960), 824–828. https://doi.org/10.1038/nature02038

Hendrawan, I. G., Asai, K., Triwahyuni, A., and Lestari, D. V. (2019): The interanual rainfall variability in Indonesia corresponding to El Niño Southern Oscillation and Indian Ocean Dipole. Acta Oceanologica Sinica, 38(7), 57–66. https://doi.org/10.1007/s13131-019-1457-1

Hendrizan, M., Kuhnt, W., and Holbourn, A. (2017): Variability of Indonesian Throughflow and Borneo Runoff During the Last 14 kyr. Paleoceanography, 32(10), 1054–1069. https://doi.org/10.1002/2016PA003030

Holbourn, A., Kuhnt, W., Kawamura, H., Jian, Z., Grootes, P., Erlenkeuser, H., and Xu, J. (2005): Orbitally paced paleoproductivity variations in the Timor Sea and Indonesian throughflow variability during the last 460 kyr. Paleoceanography,20(3),1–18.https://doi.org/10.1029/2004PA001094

Holbourn, A., Kuhnt, W., and Xu, J. (2011): Indonesian Throughflow variability during the last 140 ka: The timor sea outflow, Geological Society Special Publication, 355, 283–303. https://doi.org/10.1144/SP355.14

Huang, E., Tian, J., and Liu, J. (2015): Dynamics of the Australian-Indonesian monsoon across Termination II: Implications of molecular-biomarker reconstructions from the Timor Sea. Palaeogeography, Palaeoclimatology, Palaeoecology, 423, 32–43. https://doi.org/10.1016/j.palaeo.2015.01.027

Ishiwa, T., Yokoyama, Y., Reuning, L., McHugh, C. M., De Vleeschouwer, D., and Gallagher, S. J. (2019): Australian Summer Monsoon variability in the past 14,000 years revealed by IODP Expedition 356 sediments. Progress in Earth and Planetary Science, 6(1). https://doi.org/10.1186/s40645-019-0262-5

Kawamura, H., Holbourn, A., and Kuhnt, W. (2006): Climate variability and land-ocean interactions in the Indo Pacific Warm Pool: A 460-ka palynological and organic geochemical record from the Timor Sea. Marine Micropaleontology, 59(1), 1–14. https://doi.org/10.1016/j.marmicro.2005.09.001

Kenneth, J. P., and Srinivasan, M. S. (1983): Neogene planktonic foraminifera: A phylogenetic atlas. The Journal of Foraminiferal Research, Hutchinson and Ross, Stroudburg, Pennsylvania, 160-125.

Kuhnt, W., Holbourn, A., Hall, R., Zuvela, M., and Käse, R. (2004): Neogene history of the indonesian throughflow,

299–320 in Geophysical Monograph Series. https://doi.org/10.1029/149GM16

Kuhnt, W., Holbourn, A., Xu, J., Opdyke, B., Deckker, P. De, and Mudelsee, M. (2015): Southern Hemisphere control on Australian monsoon variability during the late deglaciation and Holocene. https://doi.org/10.1038/ncomms6916

Kusuma, D. W., Murdimanto, A., Aden, L. Y., Sukresno, B., Jatisworo, D., and Hanintyo, R. (2017): Sea Surface Temperature Dynamics in Indonesia. IOP Conference Series: Earth and Environmental Science, 98(1). https://doi.org/10.1088/1755-1315/98/1/012038

Kwiatkowski, C., Prange, M., Varma, V., Steinke, S., Hebbeln, D., and Mohtadi, M. (2015): Holocene variations of thermocline conditions in the eastern tropical Indian Ocean, Quaternary Science Reviews, 114, 33–42. https://doi.org/10.1016/j.quascirev.2015.01.028

Lana, A. B., Kurniawati, N., Purba, N. P., and Syamsuddin, M. L. (2017): Thermocline Layers Depth and Thickness in Indonesian Waters when Souteast Monsoon. Omni-Akuatika, 13(2), 65–72. https://doi.org/10.20884/1.oa.2017.13.2.70

Levi, C., Labeyrie, L., Bassinot, F., Guichard, F., Cortijo, E., Waelbroeck, C., Caillon, N., Duprat, J., de Garidel-Thoron, T., and Elderfield, H. (2007): Low-latitude hydrological cycle and rapid climate changes during the last deglaciation. Geochemistry, Geophysics, Geosystems, 8(5), 1–11. https://doi.org/10.1029/2006GC001514

Lückge, A., Mohtadi, M., Rühlemann, C., Scheeder, G., Vink, A., Reinhardt, L., and Wiedicke, M. (2009): Monsoon versus ocean circulation controls on paleoenvironmental conditions off southern Sumatra during the past 300,000 years. Paleoceanography, 24(1). https://doi.org/10.1029/2008PA001627

Lynch-Stieglitz, J., Schmidt, M. W., Gene Henry, L., Curry, W. B., Skinner, L. C., Mulitza, S., Zhang, R., and Chang, P. (2014): Muted change in Atlantic overturning circulation over some glacial-aged Heinrich events. Nature Geoscience, 7(2), 144–150. https://doi.org/10.1038/ngeo2045

Martínez, J. I., De Deckker, P., and Barrows, T. T. (1999): Palaeoceanography of the last glacial maximum in the eastern Indian Ocean: Planktonic foraminiferal evidence. Palaeogeography, Palaeoclimatology, Palaeoecology, 147(1–2), 73–99. https://doi.org/10.1016/S0031-0182(98)00153-9

Mohtadi, M., Max, L., Hebbeln, D., Baumgart, A., Krück, N., and Jennerjahn, T. (2007): Modern environmental conditions recorded in surface sediment samples off W and SW Indonesia: Planktonic foraminifera and biogenic compounds analyses. Marine Micropaleontology, 65(1–2), 96–112. https://doi.org/10.1016/j.marmicro.2007.06.004

Mohtadi, M., Oppo, D. W., Lückge, A., DePol-Holz, R., Steinke, S., Groeneveld, J., Hemme, N., and Hebbeln, D. (2011a): Reconstructing the thermal structure of the upper ocean: Insights from planktic foraminifera shell chemistry and alkenones in modern sediments of the tropical eastern Indian Ocean. Paleoceanography, 26(3), n/a-n/a. https://doi.org/10.1029/2011PA002132

Mohtadi, M., Oppo, D. W., Steinke, S., Stuut, J. B. W., De Pol-Holz, R., Hebbeln, D., and Lückge, A. (2011b): Glacial to Holocene swings of the Australian-Indonesian monsoon. Nature Geoscience, 4(8), 540–544. https://doi.org/10.1038/ngeo1209

Mohtadi, M., Prange, M., and Steinke, S. (2016): Palaeoclimatic insights into forcing and response of monsoon rainfall. Nature, 533(7602), 191–199. https://doi.org/10.1038/nature17450

Müller, A., and Opdyke, B. N. (2000): Glacial-interglacial changes in nutrient utilization and paleoproductivity in the Indonesian Throughflow sensitive Timor Trough, easternmost Indian Ocean. Paleoceanography, 15(1), 85–94. https://doi.org/10.1029/1999PA900046

Ningsih, N. S., Rakhmaputeri, N., and Harto, A. B. (2013): Upwelling variability along the southern coast of Bali and in Nusa Tenggara waters. Ocean Science Journal, 48(1), 49–57. https://doi.org/10.1007/s12601-013-0004-3

Potemra, J. T., Sprintall, J., Hautala, S. L., and Pandoe, W. (2003): Observed estimates of convergence in the Savu Sea, Indonesia. Journal of Geophysical Research C: Oceans, 108(1), 1–1. https://doi.org/10.1029/2002jc001507

Putra, P. S., and Nugroho, S. H. (2020): Holocene Climate Dynamics in Sumba Strait, Indonesia: A Preliminary Evidence From High Resolution Geochemical Records and Planktonic Foraminifera, Studia Quartenaria, 32(2), 91–99. https://doi.org/10.24425/sq.2020.133753

Qu, T., Du, Y., Strachan, J., Meyers, G., and Slingo, J. (2005): Sea Surface Temperature and Its Variability in the Indonesian Region. Oceanography, 18(4), 50–61. https://doi.org/10.5670/oceanog.2005.05

Ravelo, A. C., Fairbanks, R. G., and Philander, S. G. H. (1990): Reconstructing Tropical Atlantic hydrography using planktonic foraminifera and an ocean model. Paleoceanography, 5(3), 409–431.

Reimer, P. J., Edouard Bard, B., Alex Bayliss, B., Warren Beck, B. J., Paul Blackwell, B. G., and Christopher Bronk Ramsey, B. (2013): Intcal13 and Marine13 Radiocarbon Age Calibration Curves 0–50,000 Years Cal Bp. Radiocarbon, 55(4), 1869–1887. https://doi.org/10.1017/S0033822200048864

Schott, F. A., and McCreary, J. P. (2001): The monsoon circulation of the Indian Ocean. Progress in Oceanography, 51(1), 1–123. https://doi.org/10.1016/S0079-6611(01)00083-0

Setiawan, R. Y., Mohtadi, M., Southon, J., Groeneveld, J., Steinke, S., and Hebbeln, D. (2015): The consequences of opening the Sunda Strait on the hydrography of the eastern tropical Indian Ocean. Paleoceanography, 30(10), 1358–1372. https://doi.org/10.1002/2015PA002802

Solanki, S. K., Usoskin, I. G., Kromer, B., Schüssler, M., and Beer, J. (2004): Unusual activity of the Sun during recent decades compared to the previous 11,000 years. Nature, 431(7012), 1084–1087. https://doi.org/10.1038/nature02995

Spooner, M. I., Barrows, T. T., De Deckker, P., and Paterne, M. (2005): Palaeoceanography of the Banda Sea, and Late Pleistocene initiation of the Northwest Monsoon. Global and Planetary Change, 49(1–2), 28–46. https://doi.org/10.1016/j.gloplacha.2005.05.002

Sprintall, J., Potemra, J. T., Hautala, S. L., Bray, N. A., and Pandoe, W. W. (2003): Temperature and salinity variability in the exit passages of the Indonesian Throughflow. Deep-

Sea Research Part II: Topical Studies in Oceanography, 50(12–13), 2183–2204. https://doi.org/10.1016/S0967-0645(03)00052-3

Sprintall, J., and Révelard, A. (2014): The Indonesian Throughflow response to Indo-Pacific climate variability. Journal of Geophysical Research: Oceans, 119(2), 1161–1175. https://doi.org/10.1002/2013JC009533

Sprintall, J., Wijffels, S. E., Molcard, R., and Jaya, I. (2009): Direct estimates of the indonesian throughflow entering the indian ocean: 2004-2006. Journal of Geophysical Research: Oceans, 114(7), 2004–2006. https://doi.org/10.1029/2008JC005257

Steinke, S., Mohtadi, M., Prange, M., Varma, V., Pittauerova, D., and Fischer, H. W. (2014a): Mid- to Late-Holocene Australian-Indonesian summer monsoon variability. Quaternary Science Reviews, 93, 142–154. https://doi.org/10.1016/j.quascirev.2014.04.006

Steinke, S., Prange, M., Feist, C., Groeneveld, J., and Mohtadi, M. (2014b): Upwelling variability off southern Indonesia over the past two millennia. Geophysical Research Letters, 41(21), 7684–7693. https://doi.org/10.1002/2014GL061450

Susanto, R. D., Gordon, A. L., and Zheng, Q. (2001): Upwelling along the coasts of Java and Sumatra and its relation to ENSO. Geophysical Research Letters, 28(8), 1599–1602. https://doi.org/10.1029/2000GL011844

Susanto, R. D., Moore, T. S., and Marra, J. (2006): Ocean color variability in the Indonesian Seas during the SeaWiFS era. Geochemistry, Geophysics, Geosystems, 7(5), 1–16. https://doi.org/10.1029/2005GC001009

Talma, A. S., and Vogel, J. C. (1993): A simplified approach to calibrating 14C dates. Radiocarbon, 35(2), 317–322. https://doi.org/10.1017/S0033822200065000

Wang, P. X., Wang, B., Cheng, H., Fasullo, J., Guo, Z., and Kiefer, T. (2017): Earth-Science Reviews The global monsoon across time scales : Mechanisms and outstanding issues, Earth-Science Reviews, 174(July 2016), 84–121. https://doi.org/10.1016/j.earscirev.2017.07.006

Wanner, H., Beer, J., Bütikofer, J., Crowley, T. J., Cubasch, U., Flückiger, J., Goosse, H., Grosjean, M., Joos, F., Kaplan, J. O., Küttel, M., Müller, S. A., Prentice, I. C., Solomina, O., Stocker, T. F., Tarasov, P., Wagner, M., and Widmann, M. (2008): Mid- to Late Holocene climate change: an overview. Quaternary Science Reviews, 27(19–20), 1791–1828. https://doi.org/10.1016/j.quascirev.2008.06.013

Wheeler, M. C., and McBride, J. L. (2005): Australian-Indonesian monsoon, 125–173 in Intraseasonal Variability in the Atmosphere-Ocean Climate System, Springer Berlin Heidelberg, Berlin, Heidelberg. https://doi.org/10.1007/3-540-27250-X_5

Wyrwoll, K. H., and Miller, G. H. (2001): Initiation of the Australian summer monsoon 14,000 years ago. Quaternary International, 82(85), 119–128. https://doi.org/10.1016/S1040-6182(01)00034-9

Xu, J. (2014): Change of Indonesian Throughflow outflow in response to East Asian monsoon and ENSO activities since the Last Glacial. Science China Earth Sciences, 57(4), 791–801. https://doi.org/10.1007/s11430-014-4845-0

Xu, J., Holbourn, A., Kuhnt, W., Jian, Z., and Kawamura, H. (2008): Changes in the thermocline structure of the Indonesian out fl ow during Terminations I and II. Earth and Planetary Science Letters 273, 152–162. https://doi.org/10.1016/j.epsl.2008.06.029

Xu, J., Kuhnt, W., Holbourn, A., Andersen, N., and Bartoli, G. (2006): Changes in the vertical profile of Indonesian Throughflow during Termination II: Evidence from the Timor Sea. Paleoceanography, 21(4), 1–14. https://doi.org/10.1029/2006PA001278

Xu, Y., Wang, L., Yin, X., Ye, X., Li, D., Liu, S., Shi, X., Troa, R. A., Zuraida, R., Triarso, E., and Hendrizan, M. (2017): The influence of the Sunda Strait opening on paleoenvironmental changes in the eastern Indian Ocean. Journal of Asian Earth Sciences, 146, 402–411. https://doi.org/10.1016/j.jseaes.2017.06.014

Yim, S. Y., Wang, B., Liu, J., and Wu, Z. (2014): A comparison of regional monsoon variability using monsoon indices. Climate Dynamics, 43(5–6), 1423–1437. https://doi.org/10.1007/s00382-013-1956-9

Zhang, P., Zuraida, R., Rosenthal, Y., Holbourn, A., Kuhnt, W., and Xu, J. (2019): Geochemical characteristics from tests of four modern planktonic foraminiferal species in the Indonesian Throughflow region and their implications. Geoscience Frontiers, 10(2), 505–516. https://doi.org/10.1016/j.gsf.2018.01.011

Zhang, P., Zuraida, R., Xu, J., and Yang, C. (2016): Stable carbon and oxygen isotopes of four planktonic foraminiferal species from core-top sediments of the Indonesian throughflow region and their significance. Acta Oceanologica Sinica, 35(10), 63–75. https://doi.org/10.1007/s13131-016-0890-1

Papers written in non-English language:

Ardi, R. D. W., Maryunani, K. A., Yulianto, E., Putra, P. S., Nugroho, S. H. (2019): Biostratigrafi dan analisis perubahan kedalaman termoklin di lepas pantai barat daya Sumba sejak Pleistosen Akhir berdasarkan kumpulan foraminifera planktonik (*Biostratigraphy and analysis of changes in thermocline depth off the Southwest Coast of Sumba since the Late Pleistocene based on planktonic foraminifera assemblages*). Buletin Geologi, 3(2), 355–362. https://doi.org/10.5614/bull.geol.2019.3.2.3. (*in Indonesian with English Abstract*)

Damanik, A., Putra, P. S., Nugroho, S. H., Kapid, R. (2019): Hubungan vertikal antara kelimpahan foraminifera dan karakteristik sedimen inti di Selat Sumba, Nusa Tenggara Timur (*The vertical relationship between foraminiferal abundance and characterisitics of core sediment in Sumba Strait, East Nusa Tenggara*). Jurnal Geologi Kelautan, 17(1), 19–32. https://doi.org/10.32693/jgk.17.1.2019.563. (*in Indonesian with English Abstract*)

Chapters in books or proceedings with editor(s):

Bolli, H. M., Saunders, J. B. (1985). Oligocene to Holocene low latitude planktic foraminifera. In H. M. Bolli, J. B. Saunders, & K. Perch-Nielsen (Eds.): Plankton Stratigraphy 1st edition. – New York: Cambridge University Press, 155–262, 1032 p.

Tomczak, M., and Godfrey, J. S. (2003): Adjacent seas of the Indian Ocean and the Australasian Mediterranian Sea (The Indonesian Throughflow) (pdf version), 215–228 in Regional Oceanography: An Introduction, Daya Publishing House, Delhi.

Books/thesis:

Maryunani (2009): Microfossil approach based on Cendrawasih Bay data, to interpreting and reconstructing Equatorial Western Pacific paleoclimate since Last Glacial (Late Pleistocene). Institut Teknologi Bandung, 141 pp.

Books/thesis written in non-English language:

Ardi, R. D. W. (2018): Rekonstruksi paleoklimatologi dan palo-oseanografi sejak Pleistosen Akhir berdasarkan kumpulan foraminifera di lepas pantai barat daya Sumba, Nusa Tenggara Timur (*Paleoclimatology and paleo-oceanography reconstruction since Late Pleistocene based on foraminiferal assemblages off the southwest coast of Sumba Island*), East Nusa Tenggara. Institut Teknologi Bandung, 65 pp. (*in Indonesian with English Abstract*)

Internet sources:

GEBCO Bathymetric Compilation Group 2020 (2020): GEBCO_2020 Grid. URL: https://www.gebco.net/data_and_products/gridded_bathymetry_data (accessed 22nd July 2020)

Blaauw, M. (2020): clam: Classical Age-Depth Modelling of Cores from Deposits. R package version 2.3.4. URL: http://cran.r-project.org/package=clam (accessed 24th August 2020)

R Core Team. (2013). R: A language and environment for statistical computing. Vienna, Austria: R Foundation for Statistical Computing. URL: http://www.r-project.org (accessed 21st August 2020)

SAŽETAK

Dubina promjene termoklina na otoku Sumba na temelju planktonskih sklopova foraminifera i njegove implikacije na eutrofikaciju od posljednje deglacijacije (~ 18 ka BP): preliminarna studija

Područje ispitivanja nalazi se uz otok Sumba, a promjene dubine termokline (DOT) u ovoj regiji nisu dobro poznate u usporedbi s Timorskim morem. Zajednice planktonskih foraminifera korištene su za prepoznavanje DOT-a i promjene paleoproduktivnosti u jezgrama prikupljenim s jugozapadne Sumbe (ST08) i iz tjesnaca Sumba (ST12, ST13 i ST14). Ova studija sugerira da su tisućljetne promjene u režimu australsko-indonezijskoga monsuna (AIM) bile glavni čimbenik DOT promjena na jugozapadu Sumbe i tjesnaca Sumba nakon posljednje deglacijacije, što je stvorilo suprotne uvjete u odnosu na Timorsko more. Učinak poput južnih oscilacija *El Niño* (ENSO) i dipola Indijskoga oceana (IOD) sličnih DOT promjenama naznačen je samo oko kasnoga holocena, dok su promjene indonezijskoga protoka (ITF) utjecale samo na istočni tjesnac Sumba oko srednjega i kasnoga holocena. Produbljavanje termokline usko je povezano s poboljšanjem AIWM (AISM), *El Niñom* (*La Niñom*) i pozitivnim (negativnim) IOD-om. Poboljšanje paleoproduktivnosti nije bilo povezano samo s jačanjem DOT-a, već i s većom dostupnošću hranjivih sastojaka zbog povećanoga donosa slatke vode rijekama. Promjene u prirodi podignute vodene mase također su utjecale na promjene u paleoproduktivnosti.

Ključne riječi:
australsko-indonezijski monsun, primijenjena mikropaleontologija, indonezijski protok, Mali Sundski otoci, paleoceanografija

Author's contribution

Ryan Dwi Wahyu Ardi (1) (M. Sc., intern researcher, doctoral candidate, applied micropaleontologist, quarternary geologist) as the main contributor provided the micropaleontological analysis, paleoenvironmental interpretation, age-depth modeling, and presentation of the results. **Aswan (2)** (Dr., associate professor, quarternary geologist, paleontologist) provided the paleoenvironmental interpretation and presentation of the results. **Khoiril Anwar Maryunani (3)** (Dr., assistant professor, applied micropaleontologist, paleoclimatologist, paleoceanographer) provided paleoenvironmental interpretation and paleoclimatological and paleoceanographic views. **Eko Yulianto (4)** (Dr., senior researcher, quarternary geologist, paleoclimatologist) provided the paleoenvironmental interpretation and administered the research. **Purna Sulastya Putra (5)** (M. Sc., senior researcher, doctoral candidate, quarternary geologist, marine geologist) performed fieldwork and provided the regional marine geology view. **Septriono Hari Nugroho (6)** (M. Sc., junior researcher, doctoral candidate, quarternary geologist, marine geologist) performed the fieldwork and provided the regional marine geology view.

Supplementary Material 1
ST08 Planktonic Foraminifera Distribution

Num.	Depth interval (cm)		Age (ka BP)	Epoch	Low latitude planktonic foraminifera zone (Bolli and Saunders, 1985)	Biostratigraphic event	*Globorotalia fimbriata* biostratigraphic range	Total planktonic foraminifera	Thermocline dwellers (*Pulleniatina obliqueloculata*, *Neogloboquadrina* spp., and *Globorotalia* spp.)	Thermocline dwellers relative abundance (%)	Thermocline dwellers relative abundance smoothed (%)*	Mixed layer dwellers (*Globigerinoides ruber* , *Globigerinoides trilobus* , and other *Globigerinoides* taxa)	Mixed layer dwellers relative abundance (%)	Mixed layer dwellers relative abundance smoothed (%)*	*Neogloboquadrina dutertrei*	*Neogloboquadrina dutertrei relative abundance (%)*	Neogloboquadrina dutertrei relative abundance smoothed (%)*
	Top	Bottom															
1	0	1	-0.066	Holocene	*Globorotalia truncatulinoides* zone	*Globorotalia fimbriata* subzone		449	306	68.246	68.246	91	20.331	20.331	50	11.199	11.199
2	2	3	0.197					583	476	81.647	71.597	51	8.748	17.435	100	17.153	12.688
3	4	5	0.460					392	260	66.176	70.242	88	22.549	18.714	81	20.588	14.663
4	6	7	0.723					774	619	79.878	72.651	81	10.427	16.642	137	17.697	15.421
5	8	9	0.986					492	342	69.542	71.873	104	21.081	17.752	81	16.409	15.668
6	10	11	1.249					459	337	73.295	72.229	72	15.602	17.215	120	26.125	18.282
7	12	13	1.513					683	498	72.948	72.409	117	17.104	17.187	136	19.895	18.686
8	14	15	1.776					579	430	74.330	72.889	74	12.705	16.067	85	14.693	17.687
9	16	17	2.039					792	661	83.520	75.547	91	11.441	14.910	95	12.059	16.280
10	18	19	2.302					964	711	73.792	75.108	154	16.015	15.186	133	13.836	15.669
11	20	21	2.565					503	339	67.432	73.189	114	22.734	17.073	85	16.858	15.966
12	22	23	2.828					550	384	69.809	72.344	112	20.460	17.920	74	13.539	15.360
13	24	25	3.091					726	495	68.170	71.301	122	16.842	17.650	109	14.988	15.267
14	26	27	3.172					1186	823	69.395	70.824	233	19.627	18.145	251	21.171	16.743
15	28	29	3.252					675	353	52.380	66.213	195	28.842	20.819	113	16.801	16.757
16	30	31	3.333					635	374	58.796	64.359	144	22.685	21.285	82	12.963	15.809
17	32	33	3.414					355	245	69.014	65.523	82	23.005	21.715	52	14.554	15.495
18	34	35	3.494					575	381	66.171	65.685	128	22.237	21.846	128	22.218	17.176
19	36	37	3.575					835	547	65.508	65.641	177	21.223	21.690	175	20.897	18.106
20	38	39	3.656					711	448	63.071	64.998	149	21.011	21.520	97	13.697	17.004
21	40	41	3.736					650	489	75.314	67.577	88	13.553	19.529	128	19.647	17.665
22	42	43	3.817					586	422	71.993	68.681	110	18.825	19.353	148	25.253	19.562
23	44	45	3.898					563	402	71.534	69.394	123	21.785	19.961	117	20.810	19.874
24	46	47	3.978					1010	695	68.834	69.254	210	20.781	20.166	212	21.012	20.158
25	48	49	4.059					660	461	69.821	69.396	125	19.007	19.876	58	8.778	17.313
26	50	51	4.140					795	507	63.713	67.975	160	20.122	19.938	114	14.369	16.577
27	52	53	4.220					821	610	74.239	69.541	124	15.046	18.715	116	14.159	15.972
28	54	55	4.301					762	488	64.093	68.179	134	17.595	18.435	158	20.754	17.168
29	56	57	4.382					903	597	66.039	67.644	177	19.582	18.722	142	15.744	16.812
30	58	59	4.462					991	600	60.575	65.877	240	24.180	20.086	178	17.920	17.089
31	60	61	4.543					1597	1129	70.728	67.090	208	13.028	18.322	413	25.838	19.276
32	62	63	4.623					1331	1100	82.645	70.978	131	9.842	16.202	272	20.452	19.570
33	64	65	4.704					982	706	71.895	71.208	147	14.924	15.882	224	22.767	20.369
34	66	67	4.785					996	723	72.621	71.561	138	13.860	15.377	223	22.404	20.878
35	68	69	4.865					811	471	58.051	68.183	205	25.259	17.847	106	13.061	18.924
36	70	71	4.946					1005	611	60.810	66.340	223	22.199	18.935	253	25.150	20.480
37	72	73	5.027					2547	1495	58.691	64.428	610	23.950	20.189	326	12.813	18.563
38	74	75	5.107					2080	1355	65.160	64.611	420	20.189	20.189	352	16.941	18.158
39	76	77	5.220					2758	1765	64.021	64.463	472	17.113	19.420	563	20.412	18.721
40	77	78	5.276					2067	1340	64.836	64.556	405	19.595	19.464	407	19.708	18.968
41	78	79	5.332					513	307	59.850	63.380	105	20.470	19.715	81	15.774	18.170
42	79	80	5.388					1107	697	62.934	63.268	180	16.221	18.842	217	19.642	18.538
43	80	81	5.444					2154	1429	66.329	64.034	372	17.263	18.447	390	18.130	18.436
44	82	83	5.556					984	604	61.382	63.371	204	20.732	19.018	232	23.577	19.721
45	84	85	5.668					1267	956	75.399	66.378	173	13.642	17.674	250	19.726	19.722
46	86	87	5.781					1231	909	73.844	68.244	220	17.870	17.723	291	23.630	20.699
47	88	89	5.893					1866	1339	71.778	69.128	273	14.652	16.955	270	14.449	19.137
48	90	91	6.005					1614	1222	75.731	70.779	242	14.974	16.460	406	25.129	20.635
49	92	93	6.117					884	545	61.669	68.501	150	16.997	16.594	168	19.001	20.226
50	94	95	6.229					1155	898	77.729	70.808	151	13.061	15.711	302	26.155	21.709
51	96	97	6.342					912	639	70.117	70.635	158	17.372	16.126	187	20.510	21.409
52	98	99	6.454					1153	758	65.748	69.414	198	17.206	16.396	189	16.437	20.166
53	100	101	6.566					1368	1039	75.927	71.042	167	12.210	15.349	310	22.637	20.784
54	102	103	6.678					1439	1008	70.045	70.793	207	14.389	15.109	306	21.300	20.913
55	104	105	6.790					2415	1755	72.657	71.259	283	11.736	14.266	462	19.109	20.462
56	106	107	7.003					1802	1285	71.279	71.264	256	14.209	14.252	315	17.500	19.721
57	108	109	7.216					1111	812	73.084	71.719	157	14.097	14.213	372	33.513	23.169
58	110	111	7.428					1447	1003	69.358	71.129	255	17.660	15.075	320	22.136	22.911
59	112	113	7.641					1459	1013	69.448	70.709	245	16.804	15.507	288	19.741	22.119
60	114	115	7.853					923	658	71.217	70.836	154	16.668	15.797	186	20.191	21.637
61	116	117	8.066					1189	823	69.264	70.443	225	18.913	16.576	163	13.696	19.651
62	118	119	8.279					1455	943	64.819	69.037	288	19.787	17.379	301	20.661	19.904
63	120	121	8.491					1054	604	57.336	66.112	184	17.502	17.410	157	14.850	18.640
64	122	123	8.704					1150	675	58.742	64.269	210	18.286	17.629	223	19.362	18.821
65	124	125	8.916					985	570	57.871	62.670	195	19.799	18.171	143	14.564	17.756
66	126	127	9.129					1775	1166	65.669	63.420	244	13.736	17.062	290	16.320	17.397
67	128	129	9.342					1842	1129	61.294	62.888	339	18.392	17.395	355	19.264	17.864
68	130	131	9.554					2073	1276	61.551	62.554	346	16.707	17.223	279	13.474	16.766
69	132	133	9.767					2170	1277	58.839	61.625	365	16.842	17.128	289	13.337	15.909
70	134	135	9.979					1372	715	52.087	59.241	282	20.552	17.984	216	15.742	15.867
71	136	137	10.192					1906	1112	58.347	59.017	337	17.668	17.905	229	11.992	14.898
72	138	139	10.405					1763	1063	60.267	59.330	288	16.336	17.513	269	15.244	14.985
73	140	141	10.617					1658	1070	64.577	60.641	237	14.283	16.705	250	15.057	15.003
74	142	143	10.830					1377	788	57.221	59.786	261	18.937	17.263	239	17.340	15.587
75	144	145	11.042					2006	1035	51.615	57.744	351	17.494	17.321	298	14.859	15.405
76	146	147	11.255			*Globorotalia fimbriata*		1568	1149	73.296	61.632	232	14.819	16.695	322	20.513	16.682
77	148	149	11.468	Pleistocene	*rinella calida* subzone			1927	1363	70.734	63.907	275	14.274	16.090	348	18.068	17.028
78	150	151	11.680					1740	1251	71.902	65.906	209	12.039	15.077	502	28.834	19.980
79	152	153	11.893					631	496	78.581	69.075	59	9.329	13.640	132	20.979	20.230
80	154	155	12.105					996	692	69.556	69.195	123	12.320	13.310	229	23.022	20.928
81	156	157	12.318					1074	888	82.661	72.561	69	6.439	11.592	249	23.163	21.487
82	158	159	12.531					1017	733	72.114	72.450	180	17.683	13.115	246	24.153	22.153
83	160	161	12.743					2290	1758	76.766	73.529	229	9.998	12.336	697	30.442	24.225
84	162	163	12.956					1187	943	79.438	75.006	112	9.445	11.613	367	30.893	25.892
85	164	165	13.168					2263	1817	80.292	76.327	206	9.103	10.986	696	30.756	27.108
86	166	167	13.381					1380	1046	75.787	76.192	162	11.730	11.172	437	31.652	28.244
87	168	169	13.525					1726	1345	77.973	76.637	162	9.383	10.725	524	30.346	28.770
88	170	171	13.670					1168	897	76.747	76.665	122	10.468	10.661	458	39.202	31.378
89	172	173	13.814					1860	1386	74.531	76.131	239	12.861	11.211	628	33.743	31.969
90	174	175	13.958					1105	773	70.006	74.600	151	13.699	11.833	320	28.968	31.219
91	176	177	14.102					1502	1163	77.424	75.306	117	7.782	10.820	489	32.548	31.551
92	178	179	14.247					1414	1051	74.307	75.056	151	10.689	10.787	434	30.723	31.344
93	180	181	14.391					1537	1220	79.375	76.136	130	8.480	10.210	420	27.326	30.339
94	182	183	14.535					1561	1237	79.247	76.914	151	9.650	10.070	443	28.387	29.851
95	184	185	14.679					1569	1144	72.911	75.913	144	9.197	9.852	337	21.471	27.756
96	186	187	14.824					1571	1182	75.218	75.739	157	9.996	9.888	444	28.287	27.889
97	188	189	14.968					2606	1894	72.693	74.978	272	10.433	10.024	604	23.169	26.709
98	190	191	15.112					1475	1098	74.475	74.852	124	8.380	9.613	359	24.365	26.123
99	192	193	15.256					1320	1060	80.303	76.215	127	9.596	9.609	393	29.798	27.042
100	194	195	15.401					665	479	72.106	75.188	87	13.132	10.490	158	23.846	26.243
101	196	197	15.545					1487	1000	67.249	73.203	244	16.418	11.972	371	24.978	25.927
102	198	199	15.689					1040	726	69.839	72.362	173	16.665	13.145	218	20.918	24.675

103	200	201	15.833			*Globige*			1902	1549	81.434	74.630	179	9.391	12.207	553	29.056	25.770
104	202	203	15.978						2133	1775	83.216	76.777	164	7.700	11.080	588	27.543	26.213
105	204	205	16.122						2478	2011	81.157	77.872	237	9.543	10.696	880	35.506	28.537
106	206	207	16.266						3918	3113	79.460	78.269	458	11.680	10.942	1328	33.900	29.878
107	208	209	16.410						2414	1869	77.430	78.059	290	12.025	11.213	749	31.032	30.166
108	210	211	16.555						1314	931	70.850	76.257	259	19.670	13.327	439	33.429	30.982
109	212	213	16.699						1674	1216	72.657	75.357	246	14.717	13.674	513	30.662	30.902
110	214	215	16.843						2466	2015	81.681	76.938	154	6.247	11.818	1042	42.249	33.739
111	216	217	16.988						1949	1626	83.443	78.564	145	7.436	10.722	603	30.946	33.041
112	218	219	17.132						2273	1872	82.343	79.509	167	7.364	9.883	619	27.226	31.587
113	220	221	17.276						2879	2576	89.483	82.003	91	3.148	8.199	1051	36.495	32.814
114	222	223	17.420						3220	2836	88.073	83.520	209	6.476	7.768	1120	34.778	33.305
115	224	225	17.565						3352	2701	80.572	82.783	423	12.610	8.979	1371	40.910	35.206
116	226	227	17.709						1761	1396	79.286	81.909	140	7.964	8.725	730	41.436	36.764
117	228	229	17.853						3070	2489	81.073	81.700	314	10.240	9.104	1194	38.882	37.293
118	230	231	17.997						1510	1221	80.866	81.492	118	7.784	8.774	650	43.034	38.729
119	232	233	18.142				*Globorotalia truncatulinoides,*		2561	2227	86.982	82.864	173	6.766	8.272	928	36.242	38.107
120	234	235	18.286				*Globogerinella calida* →		5912	5072	85.787		488	8.257		2633	44.543	

*Smoothed values are calculated by exponential smoothing (damping factor: 0.7)

↳ First Occurrence

→ Occurrence

Supplementary Material 2
ST12 Planktonic Foraminifera Distribution

Num.	Depth interval (cm)		Epoch	Low latitude planktonic foraminifera zone (Bolli and Saunders, 1985)		Biostratigraphic event	*Globorotalia fimbriata* biostratigraphic range	Total planktonic foraminifera	Thermocline dwellers (*Pulleniatina obliqueloculata, Neogloboquadrina* spp., and *Globorotalia* spp.)	Thermocline dwellers relative abundance (%)	Thermocline dwellers relative abundance smoothed (%)*	Mixed layer dwellers (*Globigerinoides ruber* , *Globigerinoides trilobus* , and other *Globigerinoides* taxa)	Mixed layer dwellers relative abundance (%)	Mixed layer dwellers relative abundance smoothed (%)*	*Neogloboquadrina dutertrei*	*Neogloboquadrina dutertrei relative abundance (%)*	Neogloboquadrina dutertrei relative abundance smoothed (%)*
	Top	Bottom															
1	3	4	Holocene	*Globorotalia truncatulinoides* zone	*Globorotalia fimbriata* subzone			308	223	72.403	72.403	55	24.664	24.664	25	8.117	8.117
2	7	8						303	238	78.548	74.246	48	20.168	23.315	31	10.231	8.751
3	11	12						299	234	78.261	75.451	48	20.513	22.474	32	10.702	9.336
4	15	16						296	223	75.338	75.417	44	19.731	21.651	18	6.081	8.360
5	19	20						300	238	79.333	76.592	41	17.227	20.324	20	6.667	7.852
6	23	24						302	246	81.457	78.051	33	13.415	18.251	16	5.298	7.086
7	27	28						299	240	80.268	78.716	38	15.833	17.526	23	7.692	7.268
8	31	32						294	212	72.109	76.734	51	24.057	19.485	31	10.544	8.251
9	35	36						298	242	81.208	78.076	29	11.983	17.235	26	8.725	8.393
10	39	40						296	214	72.297	76.343	54	25.234	19.634	17	5.743	7.598
11	43	44						297	233	78.451	76.975	44	18.884	19.409	12	4.040	6.531
12	47	48						300	223	74.333	76.183	45	20.179	19.640	28	9.333	7.372
13	51	52						294	226	76.871	76.389	47	20.796	19.987	33	11.224	8.527
14	55	56						290	229	78.966	77.162	46	20.087	20.017	18	6.207	7.831
15	59	60						293	217	74.061	76.232	59	27.189	22.169	14	4.778	6.915
16	63	64						295	220	74.576	75.735	55	25.000	23.018	16	5.424	6.468
17	67	68						296	214	72.297	74.704	64	29.907	25.085	8	2.703	5.338
18	71	72						310	228	73.548	74.357	68	29.825	26.507	16	5.161	5.285
19	75	76						297	204	68.687	72.656	78	38.235	30.025	8	2.694	4.508
20	79	80						302	223	73.841	73.012	60	26.906	29.089	6	1.987	3.751
21	80	81						299	219	73.244	73.081	63	28.767	28.993	9	3.010	3.529
22	81	82						299	213	71.237	72.528	61	28.638	28.886	4	1.338	2.872
23	82	83						299	209	69.900	71.740	59	28.230	28.689	10	3.344	3.013
24	83	84						297	180	60.606	68.400	78	43.333	33.083	6	2.020	2.716
25	84	85						292	148	50.685	63.085	86	58.108	40.590	5	1.712	2.415
26	88	89						304	175	57.566	61.429	78	44.571	41.785	4	1.316	2.085
27	92	93						298	189	63.423	62.027	71	37.566	40.519	5	1.678	1.963
28	96	97						300	181	60.333	61.519	78	43.094	41.292	3	1.000	1.674
29	100	101						297	187	62.963	61.952	75	40.107	40.936	1	0.337	1.273
30	104	105						303	204	67.327	63.565	66	32.353	38.361	0	0.000	0.891
31	108	109						298	211	70.805	65.737	67	31.754	36.379	1	0.336	0.724
32	112	113						295	202	68.475	66.558	66	32.673	35.267	7	2.373	1.219
33	116	117						302	219	72.517	68.346	52	23.744	31.810	9	2.980	1.747
34	120	121						298	199	66.779	67.876	57	28.643	30.860	0	0.000	1.223
35	124	125						306	186	60.784	65.748	81	43.548	34.667	9	2.941	1.739
36	128	129						301	206	68.439	66.555	62	30.097	33.296	8	2.658	2.014
37	132	133						306	210	68.627	67.177	57	27.143	31.450	22	7.190	3.567
38	136	137						307	216	70.358	68.131	64	29.630	30.904	20	6.515	4.451
39	140	141						300	216	72.000	69.292	53	24.537	28.994	26	8.667	5.716
40	144	145						293	201	68.601	69.085	56	27.861	28.654	23	7.850	6.356
41	148	149						309	192	62.136	67.000	80	41.667	32.558	26	8.414	6.974
42	152	153						304	218	71.711	68.413	57	26.147	30.634	24	7.895	7.250
43	156	157						303	208	68.647	68.483	54	25.962	29.233	12	3.960	6.263
44	160	161						302	226	74.834	70.389	61	26.991	28.560	23	7.616	6.669
45	164	165						298	208	69.799	70.212	67	32.212	29.656	29	9.732	7.588
46	168	169						296	218	73.649	71.243	54	24.771	28.190	22	7.432	7.541
47	172	173						300	222	74.000	72.070	57	25.676	27.436	18	6.000	7.079
48	176	177						301	223	74.086	72.675	43	19.283	24.990	17	5.648	6.649
49	180	181						296	211	71.284	72.258	59	27.962	25.881	13	4.392	5.972
50	184	185						299	198	66.221	70.446	63	31.818	27.662	13	4.348	5.485
51	188	189						279	183	65.591	68.990	59	32.240	29.036	28	10.036	6.850
52	192	193						290	200	68.966	68.983	56	28.000	28.725	32	11.034	8.105
53	196	197						297	214	72.054	69.904	55	25.701	27.818	22	7.407	7.896
54	200	201						297	218	73.401	70.953	41	18.807	25.115	33	11.111	8.861
55	204	205						292	209	71.575	71.140	50	23.923	24.757	21	7.192	8.360
56	208	209						297	201	67.677	70.101	53	26.368	25.241	24	8.081	8.276
57	212	213						293	194	66.212	68.934	61	31.443	27.101	24	8.191	8.251
58	216	217						301	209	69.435	69.084	68	32.536	28.732	28	9.302	8.566
59	220	221				*Globorotalia truncatulinoides,*		291	211	72.509	70.112	56	26.540	28.074	32	10.997	9.295
60	222	223				*Globorotalia fimbriata* →		289	199	68.858		56	28.141		29	10.035	

*Smoothed values are calculated by exponential smoothing (damping factor: 0.7)

→ Occurrence

Supplementary Material 3

ST13 Planktonic Foraminifera Distribution

Num.	Depth interval (cm)		Epoch	Low latitude planktonic foraminifera zone (Bolli and Saunders, 1985)		Biostratigraphic event	*Globorotalia fimbriata* biostratigraphic range	Total planktonic foraminifera	Thermocline dwellers (*Pulleniatina obliqueloculata*, *Neogloboquadrina* spp., and *Globorotalia* spp.)	Thermocline dwellers relative abundance (%)	Thermocline dwellers relative abundance smoothed (%)*	Mixed layer dwellers (*Globigerinoides ruber* , *Globigerinoides trilobus* , and other *Globigerinoides* taxa)	Mixed layer dwellers relative abundance (%)	Mixed layer dwellers relative abundance smoothed (%)*	*Neogloboquadrina dutertrei*	*Neogloboquadrina dutertrei relative abundance (%)*	Neogloboquadrina dutertrei relative abundance smoothed (%)*
	Top	Bottom															
1	0	1	Holocene	*Globorotalia truncatulinoides* zone	*Globorotalia fimbriata* subzone			223	92	41.256	41.256	68	30.493	30.493	24	10.762	10.762
2	8	9						293	83	28.328	37.377	105	35.836	32.096	23	7.850	9.889
3	16	17						239	100	41.841	38.716	67	28.033	30.877	27	11.297	10.311
4	24	25						316	102	32.278	36.785	110	34.810	32.057	36	11.392	10.636
5	32	33						296	97	32.770	35.581	97	32.770	32.271	17	5.743	9.168
6	40	41						307	87	28.339	33.408	105	34.202	32.85	17	5.537	8.079
7	48	49						276	98	35.507	34.038	83	30.072	32.017	20	7.246	7.829
8	56	57						285	92	32.281	33.511	90	31.579	31.886	21	7.368	7.691
9	64	65						304	72	23.684	30.563	113	37.171	33.471	11	3.618	6.469
10	72	73						331	109	32.931	31.273	120	36.254	34.306	21	6.344	6.432
11	80	81						283	93	32.862	31.750	106	37.456	35.251	21	7.420	6.728
12	88	89						269	89	33.086	32.151	84	31.227	34.044	11	4.089	5.937
13	96	97						280	71	25.357	30.113	102	36.429	34.759	12	4.286	5.441
14	104	105						312	78	25.000	28.579	115	36.859	35.389	14	4.487	5.155
15	112	113						293	86	29.352	28.811	110	37.543	36.035	26	8.874	6.271
16	120	121						306	89	29.085	28.893	115	37.582	36.499	21	6.863	6.448
17	128	129						319	85	26.646	28.219	111	34.796	35.988	21	6.583	6.489
18	136	137						301	79	26.246	27.627	112	37.209	36.355	22	7.309	6.735
19	144	145						298	90	30.201	28.399	75	25.168	32.999	14	4.698	6.124
20	152	153				*Globorotalia fimbriata* ↳		332	92	27.711	28.193	101	30.422	32.225	22	6.627	6.275
21	160	161	Pleistocene		*Globigerinella calida* subzone	*Globorotalia truncatulinoides*,		327	98	29.969	28.726	103	31.498	32.007	25	7.645	6.686
22	168	169				*Globigerinella calida* →		340	105	30.882		105	30.882		24	7.059	

*Smoothed values are calculated by exponential smoothing (damping factor: 0.7)

↳ First Occurrence

→ Occurrence

Supplementary Material 4

ST14 Planktonic Foraminifera Distribution

Num.	Depth interval (cm)		Epoch	Low latitude planktonic foraminifera zone (Bolli and Saunders, 1985)		Biostratigraphic event	*Globorotalia fimbriata* biostratigraphic range	Total planktonic foraminifera	Thermocline dwellers (*Pulleniatina obliqueloculata, Neogloboquadrina* spp., and *Globorotalia* spp.)	Thermocline dwellers relative abundance (%)	Thermocline dwellers relative abundance smoothed (%)*	Mixed layer dwellers (*Globigerinoides ruber* , *Globigerinoides trilobus* , and other *Globigerinoides* taxa)	Mixed layer dwellers relative abundance (%)	Mixed layer dwellers relative abundance smoothed (%)*	*Neogloboquadrina dutertrei*	*Neogloboquadrina dutertrei relative abundance (%)*	Neogloboquadrina dutertrei relative abundance smoothed (%)*
	Top	Bottom															
1	0	1	Holocene	*Globorotalia truncatulinoides* zone	*Globorotalia fimbriata* subzone			292	251	85.959	85.959	27	10.757	10.757	82	32.669	32.669
2	5	6						282	216	76.596	83.150	46	21.296	13.919	84	38.889	34.535
3	10	11						294	251	85.374	83.817	25	9.960	12.731	114	45.418	37.800
4	15	16						295	241	81.695	83.181	26	10.788	12.148	72	29.876	35.423
5	20	21						295	230	77.966	81.616	39	16.957	13.591	77	33.478	34.839
6	25	26						289	240	83.045	82.045	31	12.917	13.389	88	36.667	35.388
7	30	31						292	256	87.671	83.733	26	10.156	12.419	98	38.281	36.256
8	35	36						298	217	72.819	80.459	47	21.659	15.191	95	43.779	38.513
9	40	41						292	232	79.452	80.157	40	17.241	15.806	108	46.552	40.924
10	45	46						290	228	78.621	79.696	46	20.175	17.117	120	52.632	44.437
11	50	51						288	237	82.292	80.475	34	14.346	16.286	122	51.477	46.549
12	55	56						289	230	79.585	80.208	42	18.261	16.878	105	45.652	46.280
13	60	61						285	218	76.491	79.093	51	23.394	18.833	97	44.495	45.744
14	65	66						291	234	80.412	79.489	43	18.376	18.696	87	37.179	43.175
15	70	71						290	228	78.621	79.228	44	19.298	18.877	87	38.158	41.670
16	75	76						289	235	81.315	79.854	38	16.170	18.065	119	50.638	44.360
17	80	81						289	245	84.775	81.330	34	13.878	16.809	91	37.143	42.195
18	85	86						296	226	76.351	79.837	60	26.549	19.731	88	38.938	41.218
19	90	91						300	233	77.667	79.186	56	24.034	21.022	100	42.918	41.728
20	95	96						289	232	80.277	79.513	39	16.810	19.758	78	33.621	39.296
21	100	101						289	224	77.509	78.912	52	23.214	20.795	83	37.054	38.623
22	105	106						291	249	85.567	80.908	27	10.843	17.810	109	43.775	40.169
23	110	111						268	221	82.463	81.375	41	18.552	18.032	90	40.724	40.335
24	115	116						284	232	81.690	81.469	44	18.966	18.312	75	32.328	37.933
25	120	121				*Globorotalia fimbriata* ↳		285	229	80.351	81.134	48	20.961	19.107	102	44.541	39.916
26	125	126	Pleistocene		*Globigerinella calida* subzone			281	240	85.409	82.416	29	12.083	17.000	97	40.417	40.066
27	130	131						286	231	80.769	81.922	33	14.286	16.186	90	38.961	39.734
28	135	136						293	228	77.816	80.690	36	15.789	16.067	92	40.351	39.919
29	140	141						279	222	79.570	80.354	35	15.766	15.976	92	41.441	40.376
30	145	146						279	217	77.778	79.581	31	14.286	15.469	67	30.876	37.526
31	150	151						282	232	82.270	80.388	37	15.948	15.613	44	18.966	31.958
32	155	156				*Globigerinella calida* ↳		284	217	76.408	79.194	50	23.041	17.841	81	37.327	33.569
33	160	161						280	219	78.214	78.900	38	17.352	17.695	116	52.968	39.388
34	165	166						281	207	73.665	77.330	48	23.188	19.343	120	57.971	44.963
35	170	171						288	209	72.569	75.902	42	20.096	19.569	115	55.024	47.981
36	175	176						286	240	83.916	78.306	28	11.667	17.198	112	46.667	47.587
37	180	181						290	256	88.276	81.297	25	9.766	14.968	98	38.281	44.795
38	185	186						275	248	90.182	83.962	13	5.242	12.050	87	35.081	41.881
39	190	191						288	251	87.153	84.920	23	9.163	11.184	85	33.865	39.476
40	195	196						282	239	84.752	84.869	27	11.297	11.218	90	37.657	38.930
41	200	201						221	192	86.878	85.472	12	6.250	9.728	80	41.667	39.751
42	205	206						272	233	85.662	85.529	30	12.876	10.672	91	39.056	39.543
43	210	211						266	225	84.586	85.246	35	15.556	12.137	81	36.000	38.480
44	215	216						243	201	82.716	84.487	27	13.433	12.526	76	37.811	38.279
45	220	221						284	231	81.338	83.542	35	15.152	13.314	79	34.199	37.055
46	225	226						241	195	80.913	82.754	31	15.897	14.089	63	32.308	35.631
47	230	231						200	170	85.000	83.427	20	11.765	13.392	66	38.824	36.589
48	235	236						167	146	87.425	84.627	7	4.795	10.812	57	39.041	37.324
49	240	241				*Globorotalia truncatulinoides* →		313	252	80.511		48	19.048		93	36.905	

*Smoothed values are calculated by exponential smoothing (damping factor: 0.7)

↳ First Occurrence

→ Occurrence